MSc Thesis:

Hydraulic Modelling of the Irrigation System of Medieval Basrah

Lisa Schallwig 5005183

Thesis Committee:
Dr.Ir. Maurits Ertsen, Water Resources/Water Management
Dr.Ir. Olivier Hoes, Water Resources/Water Management
Dr.Ir. Jos Timmermans, Faculty of Technology, Policy and Management
Dr. Peter Brown, Department of History, Art History and Classics/Radboud University Nijmegen

CIE5060-09 MSc Thesis
Delft University of Technology
October 27, 2021

Abstract

Ancient Basrah has been the center of anthropological research studies due to its significance in the development of the culture, politics and economics of the region at the time. Agriculture was one of the main income revenues for ancient Basrah even though it received only an average of 60 mm of rainfall per year, indicating a large reliance on irrigation. Therefore, this study focuses on how the landscape would have offered options for irrigated farming. The unique element of this irrigation system is the existence of many large ridges, however their significance is not yet understood.

Within this study a HEC-RAS hydraulic model was set up to explore the hypothesis of the ridges themselves having served the function of elevated agricultural fields. Therefore, multiple scenarios were constructed and sensitivity analysis of the boundary conditions performed, to explore how easily the landscape within the ridge area could be flooded and transformed into a marshland. The results showed that although there were always some dry spots between the fields, most of it was flooded all day and all year round, with a mean water depth ranging from 0.3 m to 0.6 m. The maximum water depth stayed below 5 m in all model variations (except for one sensitivity analysis run), therefore the ridges (which have been hypothesized to originally have been 5 m tall) would have stayed dry.

The main limitations were set by the lack of data available. Except for the elevation data, very little data was available in general and additionally no data from before the 1940's was available. Therefore, this study should be viewed as an exploration of how the system may have functioned given certain hypothesized boundary conditions. Further research for confirmation of the utilized boundary conditions is necessary to confirm the study results, for example decreasing the river cross-sections by 25% lead to an increase in mean depth of up to 26%.

Contents

1 Introduction

1.1 Ancient Basrah

The early Islamic settlement of Basrah was founded in the 630's CE and was situated near the modern town of Zubair (Petersen, 2018). The city was one of the first urban Muslim settlements (Petersen, 2018) and developed an estimated population of 250,000, a number which was not attained again until the late twentieth century (Kennedy, 2011). Basrah was enormously important politically, economically and culturally for the emerging Islamic state, therefore it is of major importance for historical investigations (Kennedy, 2011).
Based on rough estimates of early Abbasid revenue lists, the alluvial lands of southern Iraq generated four times as much tax revenue as the next richest Islamic area, Egypt (Kennedy, 2004). These tax revenues are linked to agricultural practices, however the Basrah region only received an average of 60 mm of annual rainfall, indicating that there was a strong dependency on irrigation (Kennedy, 2011).
According to Nelson (1962) grain has always been one of the principal crops of Iraq, where barley replaces wheat in more saline soils. The growth season of barley in southern Iraq can be seen in table 1. Another main crop in this area is date palms (Nelson, 1962), which as a perennial crop would offer different conditions for successful cultivation than barley.

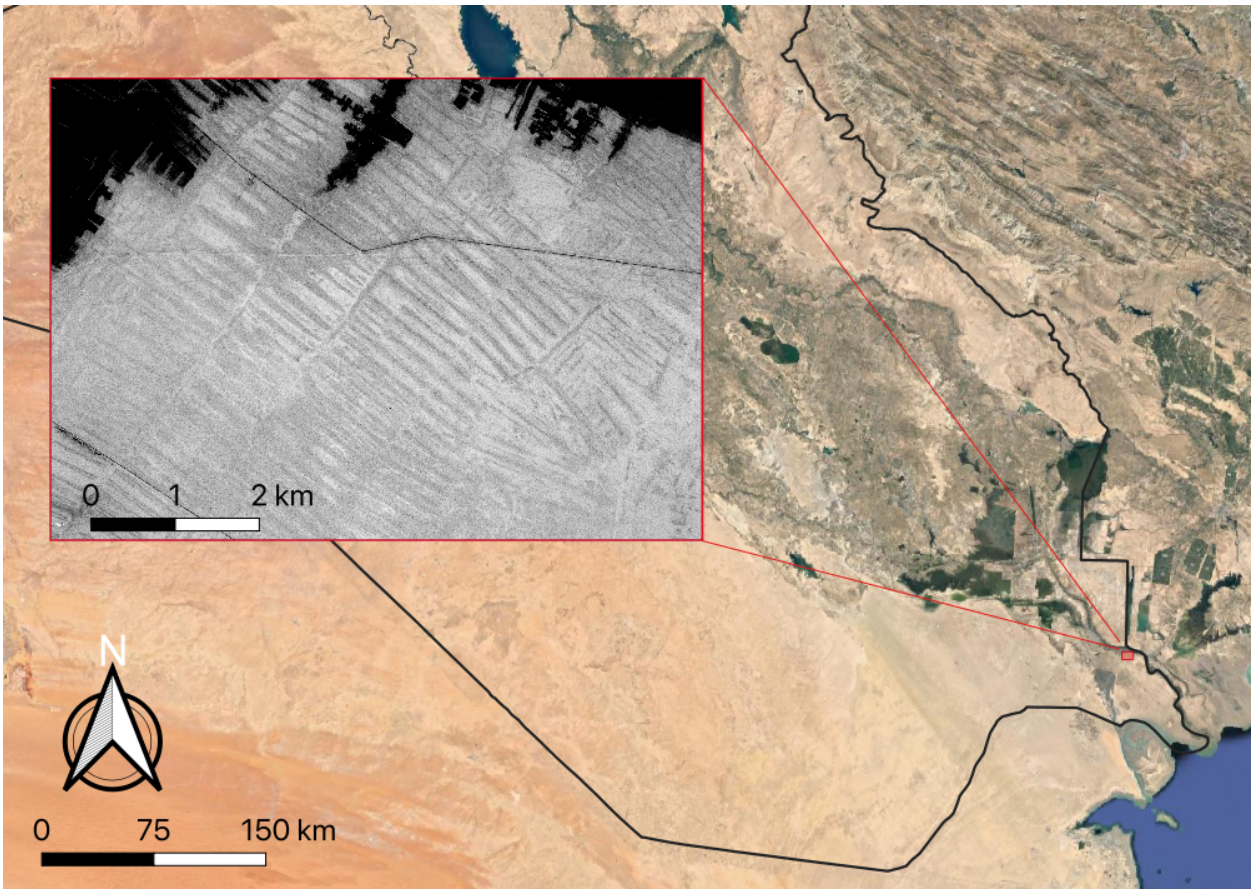

Figure 1: The location of interest in this study displayed relative to Iraq's boarders. The zoomed in map displays an excerpt of Corona satellite imagery from 1968 showing the ridge structures near ancient Basrah.

1.2 Agriculture in Ancient Basrah

A system of irrigation canals, not discernible from ground level, was detected from aerial photographs near Abul Khasib in the same area as a system of elevated ridges (Nelson, 1962), these can also be seen in figure

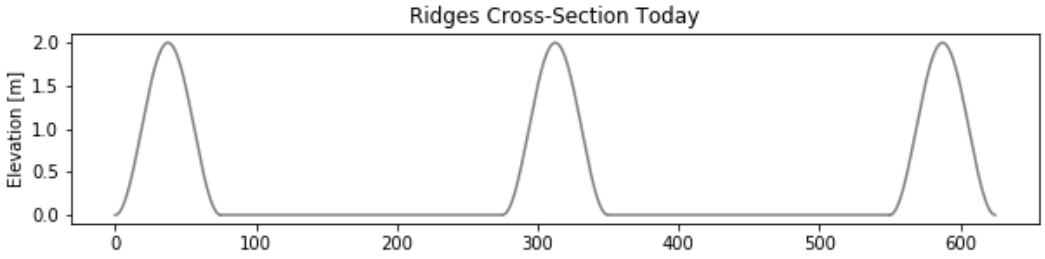

Figure 2: Schematic cross-section of the ridges in their current dimensions.

Table 1: Growth season of Barley in southern Iraq (Ewaid et al., 2019).

Month	Stage
November	Init
December	Dev
January	Mid
February	Late
March	Late

1. The ridges are an average of 1 km long, about 75 m wide, and approximately 2 m tall, spaced about 200 m apart (Nelson, 1962), for a schematic cross-section view figure 2. The soil in the elevated ridges have a higher salinity than the basins in between and there is no vegetation on the ridges, while sparse salt-resistant plants are present on the basin area (Nelson, 1962). Historians have speculated based on historical texts that the ridges were built by Zanj slaves (Nelson, 1962). The Zanj are conventionally considered to be people originating from the east coast of Africa, although there is considerable debate around the specific bounds of the Zanj's origin (Campbell, 2016). Although it is unclear when and under what circumstance the Zanj started coming, it is likely that they were imported as slaves to labour during the Umayyad and Abbasid period (Nelson, 1962). The ridges have multiple possible functionalities, two main possibilities will be discussed here. The first possibility is suggested by Nelson (1962) and states that the ridges were a response to the salinization of the topsoil. The topsoil may have been cleared in regular intervals and piled where the ridges now stand, such that the highly saline topsoil is removed and the more fertile ground beneath is revealed. The second option is that the ridges themselves were elongated fields raised above the level of the floodplain such that they were protected from floodwaters. Supporting this theory is that according to Petersen (2018) there was a marshland between the ancient city of Basrah and the ancient city of Ubulla which was situated to the east of Basrah, on the right bank of the Tigris at the head of the Persian Gulf (Kramers, 2012). The area with these ridges (from now on called "the irrigation system") would have been situated right in-between ancient Basrah and Ubulla. Such raised fields are currently in use in many parts of the world, for example in the Congo Basin and have also historically been used, for example in the Americas (Comptour, Caillon, Rodrigues, & McKey, 2018). The functioning of the raised fields varies globally; this can be based on the observation that they greatly vary in shape and dimension, some are constructed in seasonal floodplains, while others are constructed in lacustrine wetlands (Comptour et al., 2018). Raised fields can be used for both perennial and annual crops (Comptour et al., 2018). The functionality of the irrigation system of Basrah is not well understood, therefore, the objective of this study is to explore the hydraulic function of the landscape in the ridge area to help identify possible functionalities of the irrigation system.

1.3 Research Questions

The goal of this research study is to determine the likelihood of the ridges themselves being elevated fields in a marshy landscape. To determine this it will be analysed how easily the landscape in the ridge area transforms into a wetland, which will indicate the likelihood of this having been the case or not. Therefore, the main research question of this study is

In how far does the ridge system resemble a marshy area with elevated agricultural fields?

Sub-questions to help answer the main question are:

1. Where does flooding take place in the ridge system?
2. When is the ridge system flooded and how is this affected by seasonal upstream flow changes and daily tidal variations?
3. How deep is the water when the landscape is flooded and how does the depth vary throughout the landscape?
4. What does the flow pattern into and out of the ridge system look like?

To answer these questions, the next section will describe the methodology used. The methodology section includes a description of the data that was used and a description of the models simulating the possible functionalities of the landscape. The next section displays the model results along with descriptions for their various visualizations. Afterwards, in the next section, the results are discussed and interpreted. Finally, the study findings are summarized in the conclusion section.

2 Methodology

2.1 HEC-RAS

To reconstruct the landscape Hydrologic Engineering Center's River Analysis System (HEC-RAS), developed by the Hydrologic Engineering Center of the US Army Corps of Engineers was utilized. HEC-RAS has the ability to simulate 1D steady flow analysis, 1D and 2D unsteady flow analysis, sediment transport, and 1D water quality analysis (USACE HEC, 2021). To solve for 2D flow the program offers three options: 2D Diffusion Wave equations, Shallow Water Equations with a Eulerian-Lagrangian approach to solving for advection (SWE-ELM), or a new Shallow Water Equation solver that uses an Eulerian approach for advection (SWE-EM) (USACE HEC, 2021). The diffusion wave equations are the default formula used as it runs faster and is more stable (USACE HEC, 2021). These equations were used throughout this study.
HEC-RAS was chosen to perform the simulations within this study as the program is open access and because it allows a reconstruction of all features used within the simulations (1D river, 2D flow area, levee, weir, etc.). In the performed simulations both 1D and 2D flow systems were constructed. The 1D flow was utilized in the reconstruction of the river. 1D models only consider the flow velocity in one direction, which is perpendicular to the cross-sections. This means that each cross-section will be assigned one average flow velocity, but the flow velocity can vary from one cross-section to the next. In 2D flow modelling, the flow velocity in multiple directions is considered, if we stay with the example of a river, this would mean that the flow velocity could vary along one cross-section, as well as from one cross-section to the next.
The flow input data can be entered in various forms. In upstream locations a flow hydrograph, a stage hydrograph, or a flow and stage hydrograph can be given. At downstream locations a flow hydrograph, a stage hydrograph, rating curve or the normal depth can be given. Throughout this study the flow hydrograph, the stage hydrograph and the normal depth options are utilized, therefore only these three will be explained in further detail. The flow hydrograph is a dataset containing both time and date, as well as flow data for each timestamp. Further, the flow hydrograph boundary condition requires the input of an energy slope, which can be estimated by the bed slope. The stage hydrograph similarly describes a dataset with timestamps and a water-level value for each time-step. The normal depth option requires the input of only a friction slope, which is then used to estimate a stage for each computed flow. The flow is computed with the Manning's equation. The bed slope can be measured as an estimation of the friction slope. (USACE HEC, 2021)

2.2 Basic Model Setup

The hydraulic properties of the landscape of the irrigation system of ancient Basrah were explored by the use of a model in HEC-RAS 6.0 with an unsteady flow analysis. The 2D and 1D models were constructed using the RAS Mapper and the Geometric Data Editor.

Landscape Reconstruction The 2D flow area was restricted to the extended area of the ridge system, bordered by the Khor al-Zubair (the Khor al-Zubair is a city and a port northwest of the Arabian Gulf with many river branches) on the west and the Shatt Al-Arab on the east. In the north it extends to the southern edge of modern Basrah and in the south it extends to the same level of Abadan, Iran. Each side of this area, plus the part crossing the Khor al-Zubair, is separated into its own boundary and assigned a boundary condition. The boundary conditions assigned were their normal depths, which were approximated by measuring the slope at each boundary in HEC-RAS. View figure 3 for a map of the 2D flow area extent and each boundary and view table 2 for the boundary condition assigned to each boundary.

The Shatt Al-Arab was reconstructed using a 1D river structure, spanning from the Euphrates and Tigris confluence at Al-Qurna to Al-Faw. This river structure includes the centerline of the river, the bank lines, the flow path and the river cross-sections, as shown in figure 4. Figure 4b shows another variation of the river, in which the coast was changed, which will be explained in section 2.6.2. The upstream boundary was defined by a flow hydrograph and the energy slope approximated by calculating the slope between the two closest river cross-sections. The downstream boundary was defined at Al-Faw by a stage hydrograph. Table 2 shows the upstream and downstream boundary conditions and Appendices D and E show the flow and stage hydrographs used for November and July respectively.

To connect the 1D river and the 2D flow area a lateral structure was added, the width of which was set to

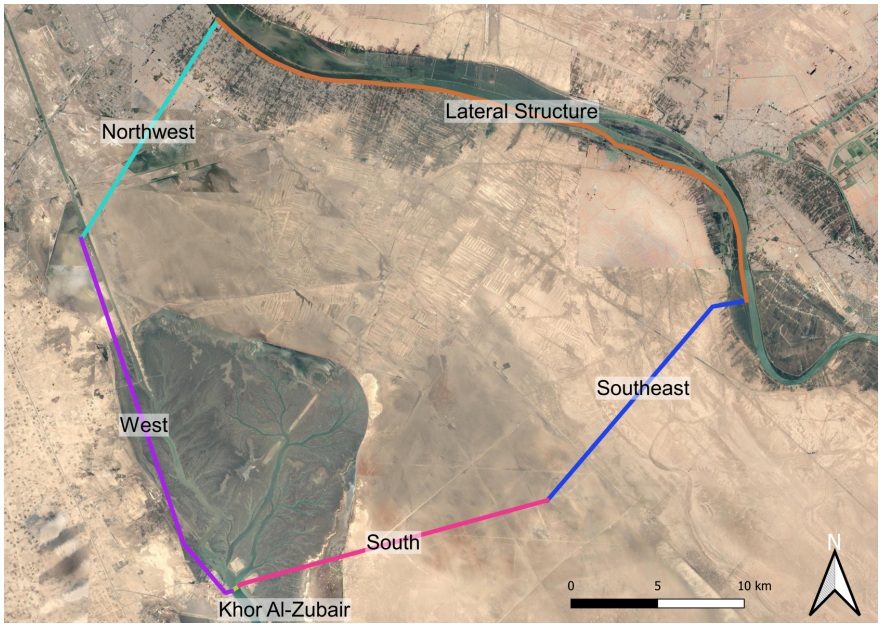

Figure 3: The boundaries of the ridge area.

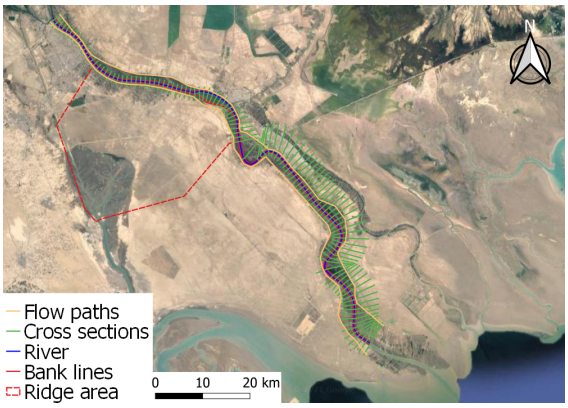

(a) River structure current coast.

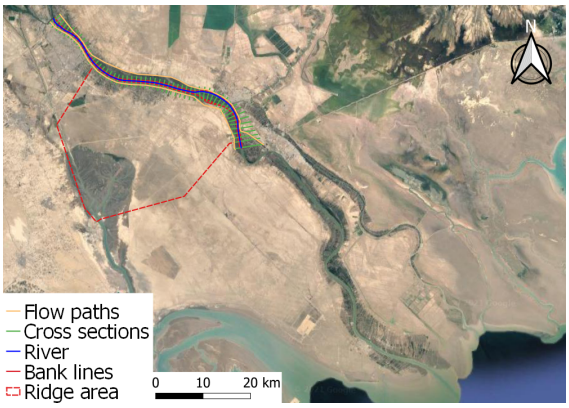

(b) River structure alternative coast.

Figure 4: Maps showing the river structures for the current and the alternative coast, respectively. The river structure includes the river centerline, the bank lines, the flow paths and the river cross-sections. Be aware that the scale varies in the two maps based on the location of the coast.

Table 2: Summary of the boundary conditions (BC). As explained in section 2.1, the normal depth boundary condition requires the input of a friction slope, which is the value displayed in this table. Energy slope and friction slope were approximated by measuring the river bed slope in HEC-RAS. NW: northwest, W: west, S: south, SE: southeast.

Location	BC	Condition 1	Condition 2
Al Qurna	Upstream	Flow hydrograph	Energy slope: 45 cm/km
Al Faw	Downstream	Stage hydrograph	
Khor al-Zubair	Downstream	Normal depth: 4 cm/km	
NW boundary of 2D Flow Area	Downstream	Normal depth: 35 cm/km	
W boundary of 2D Flow Area	Downstream	Normal depth: 9 cm/km	
S boundary of 2D Flow Area	Downstream	Normal depth: 16 cm/km	
SE boundary of 2D Flow Area	Downstream	Normal depth: 23 cm/km	

zero and the elevation was equal to the terrain elevation. Only 500 station and elevation points are allowed to be given for one lateral structure in HEC-RAS, therefore the number of data points had to be reduced, which was done with the filter function in HEC-RAS. To prevent errors from occurring, all lateral structure elevation points had to be set to be equal to or above the elevations of connected 2D cells. To do this the simulation was run, then an error message would appear with the specific station values that were too low and the level of the connected 2D cells. This information was used to edit the lateral structure elevation. The weir coefficient was set to 0.2 and the Weir Crest Shape to Zero Height as is suggested by USACE Hydrologic Engineering Center (2021a). The Tailwater Connection was of the type Storage Area/2D Flow Area. The overflow computation method was set to the normal 2D equation domain, such that the water level in the 2D area is equal to the water level in the river once the river starts overflowing its banks (USACE Hydrologic Engineering Center, 2021b). All other settings were left at their default.

The cross-sections were set up as described in section 2.5. All station and elevation points of the river cross-sections, like the lateral structure, had to be reduced to a maximum of 500 points per cross-section. To do this the filter option of the HEC-RAS Geometry Data Editor was used, which filters the data such that there is a minimum change in the area of the cross-sections.

Model Setup Based on the HEC-RAS user's manual the maximum computation time-step should be equal to the time of a rise in the hydrograph divided by 20. A python code was utilized to extract the local minima and maxima in the hydrographs shown in figure 7, the code and the resulting maxima and minima can be seen in Appendix C. The time-step computed based on the average time between a minimum and a maximum point is 20 days. However, it is important to keep in mind that this method of determining the time-step is limited by the resolution of the data set. A time-step of 30 minutes was chosen in the end, so that the simulation resolution is high enough to see gradual depth and flow changes between high and low tides.

The models were run for a period of 24 hours with a 120 hour (5 days) warm-up period for the 2D area, and 10,000 warm up time-steps, with a time-step of 0.5 hours (208.3 days) for the entire model. This specific amount of warm up time-steps was determined through an iterative process until the model was in equilibrium at the start of the simulation process.

2.3 Changes in the Boundary Conditions

Averages from 1977 - 1978 show an annual discharge of the Shatt Al-Arab of 919 m^3/s, with the Tigris contributing around 38.1%, the Euphrates contributing 30.4%, the Karun contributing 22.7% and the Karkheh contributing 8.8% (S. A. Al-Asadi & Alhello, 2019). According to Cressey (1958) the Euphrates, Tigris (here it is stated that the Karkheh converges with the Tigris above the convergence with the Euphrates) and Karun drain a total of 808,000 km^2 with a third of the basin lying in the mountains of Turkey and Iran, while most of the rest lies in the deserts of Syria and Iraq. Throughout the desert much of the water evaporates, therefore the chemical load is concentrated and may precipitate. This causes issues with salinization in irrigated fields (Cressey, 1958).

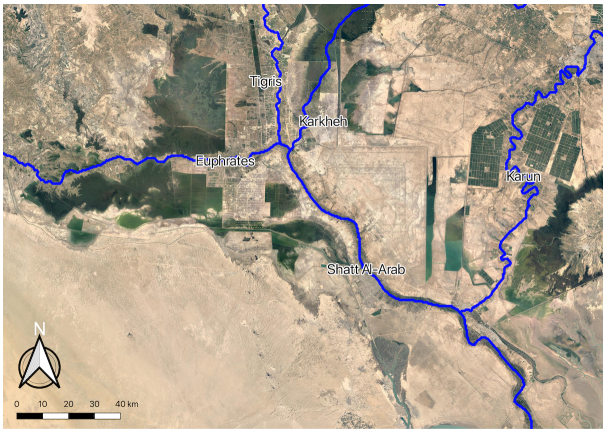

Figure 5: The Shatt Al-Arab and tributaries.

Large dam construction in the Euphrates-Tigris river system (view figure 5 for a map with the mentioned rivers) began with the turkish Keban Dam on the Euphrates in 1966. Since then increased dam construction has significantly altered the natural flow regime of the two rivers (Bremer, 2013) and consequently of the downstream Shatt Al-Arab. Nowadays, the Euphrates River has been cut off before the confluence with the Tigris and a significant amount of flow is

diverted from the Karkheh and Karun Rivers, therefore since 2010 the river depends mainly on the flow of the Tigris River (S. A. Al-Asadi & Alhello, 2019).

The downstream boundary condition is determined by the tidal influence of the Persian Gulf. Although reconstructions of the changes in the shoreline during the Holocene do exist, the most relevant reconstruction is from BCE 325 which is still about 1000 years earlier than the time period of interest in this study and can therefore only be interpreted as an indication of how the shoreline changed between BCE 325 and now. Figure 6 shows this ancient shoreline which was reconstructed by comparing localities and distances to them as well as to the shoreline, given in the account of the voyage of Nearchus as described by Strabo.
Lees and Falcon (1952) criticizes the simplistic reconstruction arguing that it does not explain the failure of the Euphrates and Tigris to silt up the Hor al Hammar (a saline lake about 40 km north west from Al Qurnah) and the marshes of the lower Tigris. Further, they show that archaeologists' simple assumption of a continuously receding shoreline does not encompass the complex system of subsidence and sedimentation as is present in the lower Mesopotamian plains, which in combination determines the migration of the shoreline. However, as no more accurate reconstruction of the shoreline for the period of interest for this study currently exists, it will still be the basis of certain assumptions made about the boundary conditions of the constructed model. It is important to keep in mind that the map is only an approximation.

Finally, boundary conditions have changed in the elevation of the terrain. As was explained above, the area is in a complicated equilibrium between subsidence and sedimentation. Further, the ridges themselves have been eroded considerably from their original form. Nelson (1962) claims that the ridges may have had dimensions of about 5 m height and 15 m width, while now they are about 2 m high and extend about 75 m. However, it is unclear how he concludes these dimensions would have been realistic. Further, he states that this spreading of the ridges may have also covered up canals which could have been in use during the time period of interest.

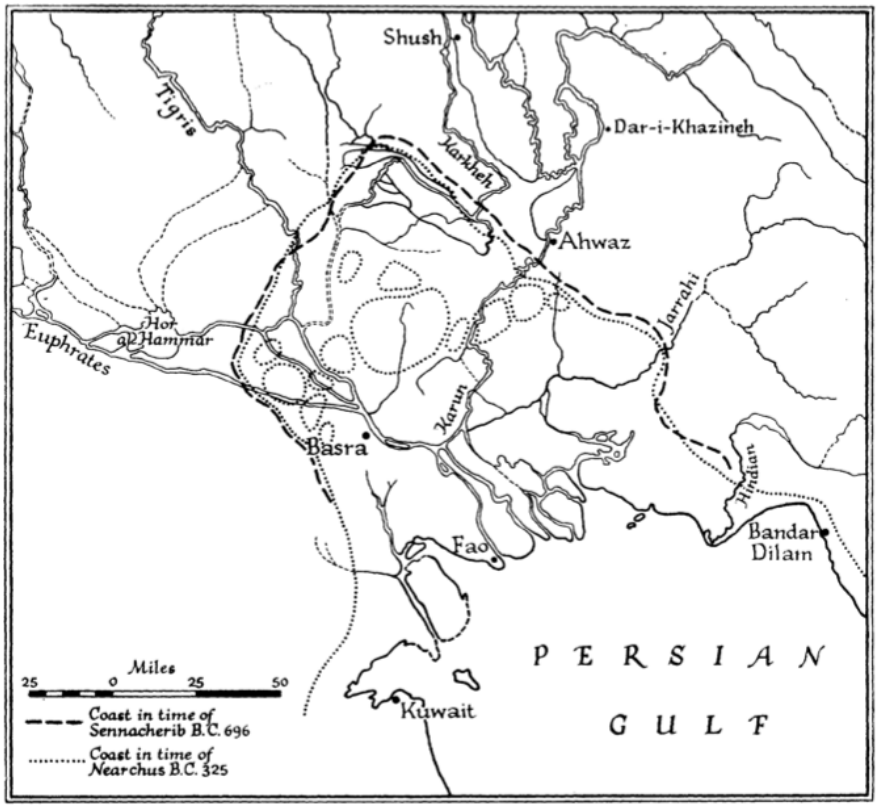

Figure 6: The historical shoreline of the Persian Gulf.
(de Morgan, 1900)

2.4 Climate and Hydrology in Iraq

Except for the north and northeastern mountainous regions of Iraq, the climate is continental and subtropical semi-arid. The winters are relatively cool, the coldest month is January which has an average temperature of 9.1 °C, while the summers are relatively hot. The hottest month is July with an average temperature of 33.5 °C. Averages were taken over the time span of 1901 to 2020. The country experiences seasonal rainfall, which, except for in the northern and northeastern region, takes place from December to February. (World Bank Group, n.d.)
The high temperatures lead to high evaporation, currently about 61% of Iraq's annual precipitation is lost to evaporation (Ali Ghorbani, Kazempour, Chau, Shamshirband, & Taherei Ghazvinei, 2018). A meteorological station in Baghdad (about 450 km northwest of Basrah), measured a yearly evaporation of 3200 mm in the period of 1999 to 2009 (Yaseen et al., 2020).

Due to snow-melt in Turkey's mountains, the flood in the Tigris occurs from March to August or September, where June is the most water abundant month, and accounts for 56–75% of the total annual runoff. The spring flood on the Euphrates occurs from April to May and carries 60-70% of the total annual runoff. (Isaev & Mikhailova, 2009)

2.5 Data in the Model

Landscape Reconstruction The digital elevation model (DEM) was sourced from the GLO-30 Copernicus mission, which acquired data in the time frame 2011 to 2015, and has a resolution of 30 m by 30 m (Fahrland, Jacob, Schrader, & Hanjo, 2020). The DEM contains elevation data of the entire area, which includes the ridges, but excludes the river bathymetry, river elevation is set to 0 m along its entire length, therefore river cross-sections had to be sourced separately. It is important to be aware of the fact that the DEM reflects the modern terrain and that there may have been differences in the terrain during the time of interest. Before the DEM could be used in HEC-RAS it had to be converted from its original projection to UTM 39N (for more information on the conversion process see Appendix A). HEC-RAS automatically sets a mannings n value of 0.06 $\frac{s}{m^{1/3}}$ to the terrain, which is a relatively higher mannings value, describing a floodplain with considerable amount of rocks or pebbles and vegetation, and is therefore considered sufficiently realistic.

On the Shatt Al-Arab river only 5 cross-sections were available, the first four are sourced from Mosawi and Muter (2019), the data was extracted using WebPlotDigitizer, the fifth was constructed from data given in Marine Science Centre: University of Basra in Cooperation with Ministry of Environment (2011). HEC-RAS also requires mannings n values to be assigned to each cross-section. These were taken from Al-Taei, Alfartusi, and Abdulhussein (2019), the harmonic mean was used. Station 1 from Mosawi and Muter (2019), was given the value from Al Sharash (not in entirely the same location, but it is the closest station), Station 2 from Mosawi and Muter (2019), was given the n value of station Ektiban given in Al-Taei et al. (2019), Station 3 was given values from Station Abeflos, Station 4 was given data from station Seehan, Station 5 was given data from Al Fao. Further cross-sections were interpolated at a distance of 1 km using HEC-RAS (for more information on this process view Appendix B). Again, it is important to stress that this is modern data describing the bathymetry of the river during the time of the respective research studies and does not accurately reflect the river bathymetry of the period of interest. Therefore, the effect of varying bathymetry was explored in the sensitivity analysis, the methods of which can be found in section 2.9.1.

Hydraulic Inputs Flow data was extracted from figure 7 using the online WebPlotDigitizer tool. This resulted in a resolution varying from 0.53 days (12 hours 43 minutes 12 seconds) to 69.0 days for the Euphrates and from 0.27 days (6 hours 28 minutes 48 seconds) to 53.5 days (53 days 12 hours) for the Tigris. As the flow data is from the 1980's, it no longer describes the natural conditions that would have been in place during the usage of the irrigation system. Table 3 shows how the flow regime has changed since before the construction of large dams. This information allows an approximation of the flow regime that would have been present while the irrigation system was in use and was later used to construct different irrigation system scenarios (view section 2.6).

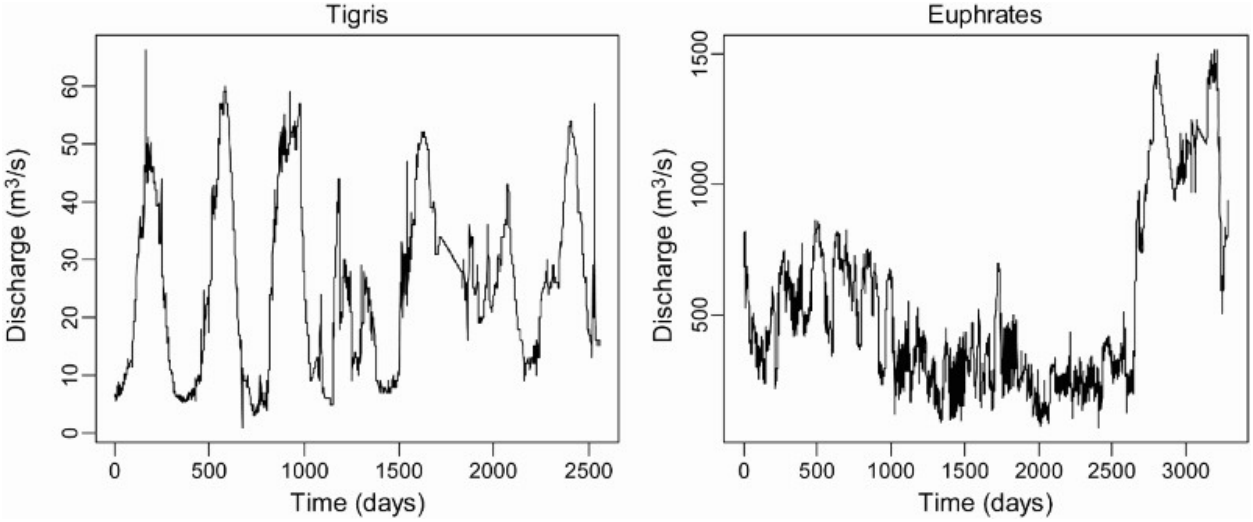

(Brandimarte, Popescu, & Neamah, 2015)

Figure 7: Flow in the Tigris from 1981 to 1987 and flow in the Euphrates from 1981 to 1989.

Table 3: Flow in the Shatt Al-Arab per month (displayed as number of month) for various time spans. Sources: [1]Al-Mahdi & Salman, 1997, [2]Ministry of Irrigation, 1979, [3]S. Al-Asadi et al., 2015, [4]Ministry of Water Resources, 2018, (S. A. Al-Asadi & Alhello, 2019).

Year	Site	Monthly Flow [m^3/s]												
		10	11	12	1	2	3	4	5	6	7	8	9	Avg.
1948 - 1960[1]	Faw	392	449	565	753	1,021	1,515	2,111	2,465	2,270	1,456	785	486	1,189
1977 - 1978[2]	Basrah	230	317	495	797	916	1,082	1,191	1,313	1,506	1,463	963	563	919
1994 - 1995[3]	Basrah	632	616	600	831	891	895	900	729	686	678	612	615	724
	Faw	834	879	-	1,039	1,064	-	725	547	-	601	826	-	815
2008 - 2008[3]	Basrah	188	197	217	256	264	295	306	301	281	263	216	164	246
	Faw	188	197	217	256	264	295	306	301	281	263	216	164	246
2017 - 2018[4]	Basrah	42	44	44	46	49	60	75	90	76	65	59	49	58
	Faw	42	44	44	46	49	60	75	90	76	65	59	49	58

It is important to note that, as can be seen in table 3 for the time period 1994-1995, the wet and dry periods experienced more similar flow volumes and were partly even reversed (see months 4, 5, and 7 at Al-Faw) from their usual pattern. The flow data from the 1980's similarly showed higher flow values in November than July, therefore, for the models based on this flow data, the wet period has the flow data from November, while the dry period is based on the flow data from July. As the objective of this study is simply to test if the ridge area was likely to be a wetland, it is currently not decisive which month a certain flow value is allocated to. However, it is more important in the interpretation of the results and the discussion of the second sub-question of the main research question, here it is important to keep in mind that the wet season usually occurs in the summer, while the dry period usually occurs in the winter.

The daily stage measurements were taken from tideschart.com for the time period of 28.06.2021 - 12.07.2021. To decrease the time step of the data, the data was linearly interpolated using Python, such that the time step was decreased to 30 minutes.

Neither evaporation, nor soil infiltration of the water was taken into consideration in this model.

Table 4: This table summarizes the decisive characteristics of each scenario set up. For a map view of the alternative coast location view figure 21 in Appendix F. The 1980's flow data can be seen in Appendix D for November and Appendix E for July. The average flow data in the period 1948 - 1960 can be seen in table 3.

Scenario	Coast	Flow data date	Simulated months	Flow [m^3/s]	
				Summer	November
1: CC80F	current	1980's	July & November	~ 460	~ 720
2: AC80F	alternative	1980's	July & November	~ 460	~ 720
3: CC60F	current	1948 - 1960	May & November	2465	449
4: AC60F	alternative	1948 - 1960	May & November	2465	449

2.6 Hydraulic Scenarios

To explore how the landscape in the ridge area may have functioned, multiple scenarios were set up and compared. The scenarios are listed below and a summary of their distinctive characteristics can be seen in table 4.

2.6.1 Scenario 1 / CC80F

The first scenario describes the hypothetical situation where no canals or any other water management structures are present and the coast is at todays location. The model includes the DEM, the 2D flow area (figure 3) and the boundary conditions shown in table 2. The model was firstly run for the start of November to visualize the available water in the wet season and in the initial growth stages of barley and then again in July to visualize the available water in the dry period. The flow data is the data from the 1980's of which the exact time-series used for the upstream flow and downstream stage boundary conditions can be seen in appendix D and E. The scenario has been given the descriptive name CC80F, which stands for **c**urrent **c**oast with 19**80**'s **f**low.

2.6.2 Scenario 2 / AC80F

Scenario 2 describes a similar system as scenario CC80F, with the singular difference of a higher coast line. As described in section 2.3 the exact position of the coast line during the period of interest is unknown, however, it can be simplistically estimated from the map by de Morgan (1900), shown in figure 6. Assuming that the extension of the coast line was steady, the location of the coast line can be linearly interpolated from the past and current position. According to this linear interpolation, the coast would be in between Basra and the Karun confluence with the Shatt Al-Arab. As this location is partly above the ridge system, part of the ridge system would be submerged in the ocean, therefore, it has instead been assumed that the coast line was just south of the ridge system. View Appendix F for the linearly interpolated and alternative location of the coast utilized in scenario 2. The location of the coastline was only extrapolated along the river, therefore the coastal location is represented as a single dot on the river in Appendix F. Within the context of this study, it was only necessary to know where the river meets the coast, and as the focus of this study is not on a detailed reconstruction of the landscape, the rest of the coast line was not interpreted.
Other than the change in coast location all boundary conditions stay the same, for the wet season the data from Appendix D is used and for the dry season the data from Appendix E is used, as in the previous scenario. The scenario has been given the descriptive name AC80F, which stands for **a**lternative **c**oast with 19**80**'s **f**low.

2.6.3 Scenario 3 / CC60F

Scenario 3 explores the situation with significantly higher flow values as was experienced before the 1960's (refer to table 3), which marks the beginning of dam construction upstream of the Shatt Al-Arab. The same model geometry as scenario CC80F was used, the difference lies in the upstream flow hydrograph, which was exchanged for a constant value of $449\,m^3/s$ in November and $2{,}465\,m^3/s$ in May, as this was the wettest month. These values were taken from table 3. For the downstream stage measurements the same values as have been used so far (as found in Appendix D for November and Appendix E for May) were used. The

scenario has been given the descriptive name CC60F, which stands for **c**urrent **c**oast with average 1948 - **60**'s **f**low.

2.6.4 Scenario 4 / AC60F

Scenario 4 is a combination of scenario AC80F and CC60F. It describes the hypothetical situation where both the coast is higher, like in scenario AC80F, and the upstream flow resembles the historical values, like in scenario CC60F. The same model geometry as in scenario AC80F and the same flow data as in model 3 were utilized. The scenario has been given the descriptive name AC60F, which stands for **c**urrent **c**oast with average 1948 - **60**'s **f**low.

2.7 Post-Processing

After the simulation of each scenario, the depth raster data was exported to QGIS 3.20.0 for post-processing. To do this the tool Zonal statistics, which can be found under Raster analysis in the Processing Toolbox, was used. The raster layer was cut with the polygon of the ridge area and then the mean, minimum and maximum values for this area were calculated. View Appendix G for the precise settings used in the zonal statistics tool.

2.8 Assumptions

During the methodology certain assumptions were made to enable the construction of a model, which may however affect the accuracy of the model.

- The first of these assumptions is that the DEM is accurate for the time of interest. This is unlikely as was discussed in section 2.3, as the ridges have eroded significantly since their original construction and the terrain and coast are in a complicated equilibrium between subsidence and sedimentation (Lees & Falcon, 1952).
- A further assumption is that the watercourse of the Shatt Al-Arab was similar at the time of interest as it is today. The watercourse having had a different shape may also affect the point of entry of the water to the ridge system and therefore the amount and distribution of water in the ridge system.
- The third assumption is that the interpolated cross-sections accurately represent the actual river cross-sections. This again is very unlikely as the measured cross-sections are on average spaced more than 10 km apart.
- The fourth assumption is that the coast can be accurately represented by the modern or the higher interpolated coast, which is again not very likely as explained in section 2.3.
- The final assumption is that the flow values of the Shatt Al-Arab were in the range of the values measured before the dam construction and the flow data of the 1980's and that the stage values were similar to the values that they are today.

The reason for making these assumptions, even though they are not an accurate representation of the system, is that this is the most accurate information that is currently available. Running simulations using the currently available data will give a first impression of how the system may have worked. Identifying the assumptions also aids in the set up of the sensitivity analysis, which will allow the identification of which parameters are most decisive for the function of the system. In consequence, further research will be able to study the most decisive parameters and either confirm the findings of this study, or implement the required corrections for higher accuracy. This is further discussed in section 5.2.

2.9 Sensitivity Analysis

One of the main goals of sensitivity analysis in general, and definitely within the context of this study, is to determine the impact of individual model parameters and therefore how many resources should be allocated towards accurately determining those parameters (Wainwright, Finsterle, Jung, Zhou, & Birkholzer, 2014).

Boundary	Original [cm/km]	Increased [cm/km]	Decreased [cm/km]
Khor al-Zubair	4	4.8	3.2
Northwest	35	42	28
West	9	10.8	7.2
South	16	19.2	12.8
Southeast	23	27.6	18.4

Table 5: The normal depth values used for the sensitivity analysis of the boundary conditions of the ridge area.

This especially applies to those parameters which are based on assumptions, as mentioned above. In this study the one-at-a-time (OAT) sensitivity analysis method was followed, which changes one parameter at a time to analyse the variation in outputs (Wainwright et al., 2014).

2.9.1 River Cross-Sections

To analyse the uncertainty of the model introduced by the approximated river cross-sections, two uncertainty analysis were performed in which the river cross-sections were increased and then decreased by 25% in area respectively. The area increase and decrease was separated evenly over the two dimensions width and depth. The model was run with the lower coast, as the interpolated coast is very speculative. The average flow data from 1948 - 1960 (view table 3) for the months November and May were utilized as these values do not include the unnatural management of flow introduced by dam construction.

2.9.2 Flow from River to Ridge Area

In the four scenarios the flow from the river to the ridge area simply went over the terrain, similarly as the flow into a floodplain. To investigate the effect of the flow style from the river into the ridge area, the terrain along the river was altered, such that the flow is more concentrated in one location. The results of Scenario CC60F for May show that the maximum water depth along the lateral structure (which is equal to the natural terrain in this case) is below 5 m (view Appendix H to see the water surface profile), therefore the terrain of the right riverbank was set to 5 m, with a weir for water inflow. The weir is located at a location where a canal is currently present and was also during the period of interest (Nelson, 1962), just east of modern Jaykur, Iraq. The weir elevation is 0 m and the width of the weir is 75.34 m, which is equal to the length of the present canal. To view the profile of the natural terrain along the lateral structure and a profile of the altered terrain, view Appendix I. Other than the altered terrain the same geometry and flow data as in scenario CC60F were utilized.
A second sensitivity analysis was run, with two inlets in the raised lateral structure (the profile can be viewed in figure 27 in Appendix I). The second inlet was added about 3.5 km downstream along the lateral structure and has a width of 78.65 m and an elevation of 0 m. The intent of this second sensitivity analysis is to investigate the transition from controlled inflow to floodplain type flow into the ridge area.

2.9.3 Boundary Conditions of the Ridge Area

As the normal depth boundary condition at the edges of the ridge area was estimated by measuring the terrain, the effect of altered boundary conditions was investigated. The boundary conditions were first increased, then decreased by 20%. The original, increased and decreased normal depths can be seen in table 5.

2.9.4 Flooding Along the Entire Shatt Al-Arab

As a consequence of the model setup, water in the Shatt Al-Arab River could only flood at the location of the ridge area. Allowing the river to flood along its entire length could have an effect on the water depth in the ridge area, therefore a sensitivity analysis simulation was set up, in which this was possible.
To build this model, a 2D flow area had to be constructed along the entire length of both the left and right

floodplain of the river. The resolution of the 2D flow area was maintained at 30 m. Additionally, the lateral structure on the right side of the river had to be extended and a lateral structure on the left side of the river had to be added as well. The lateral structures had the same settings as the lateral structure of the modeled scenarios (view section 2.2 for a description of the lateral structure settings). These additional flooding areas were not added to the four scenarios to save computation time.

3 Results

3.1 Scenarios

Figure 8 shows maps including all scenario simulation results. The figures show the minimum and maximum depth states achieved during each simulation. The figure is assorted such that the minimum and maximum depth states are displayed next to each other for one season and scenario. The left column shows the minimum depth state, while the right column shows the maximum depth state. The November simulation is presented first for each scenario and the summer simulation is presented below it. A horizontal line separates the maps into groups of one scenario. The scale varies depending on the coast location in the displayed scenario. The darkness of the blue color indicates depth, where the darkest blue color indicates 2 m depth or more and the white color shows 0 m depth. Areas in the ridge area that show the background satellite image are not flooded.

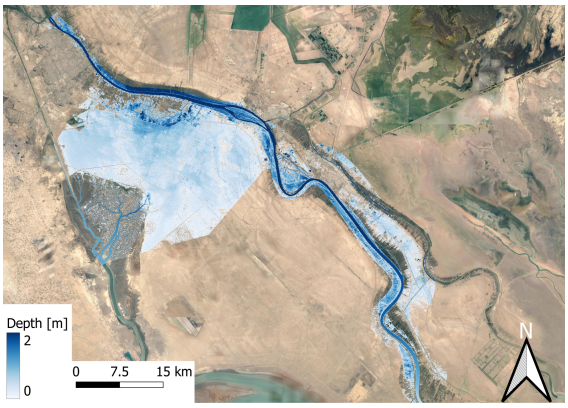

(a) Sc. CC80F, Nov., min.

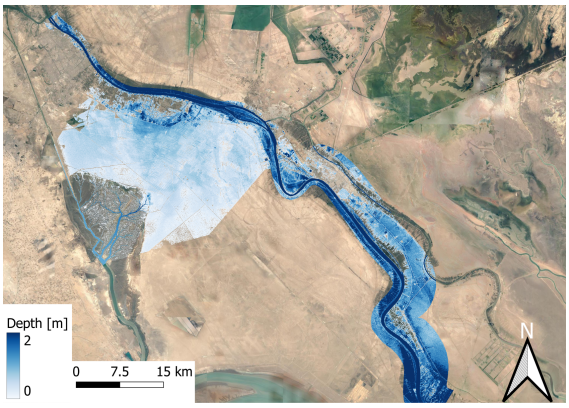

(b) Sc. CC80F, Nov., max.

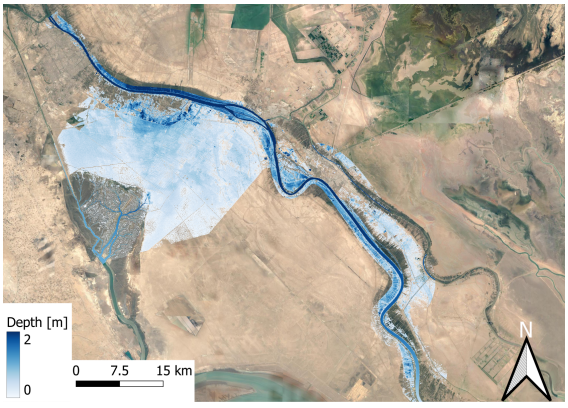

(c) Sc. CC80F, Jul., min.

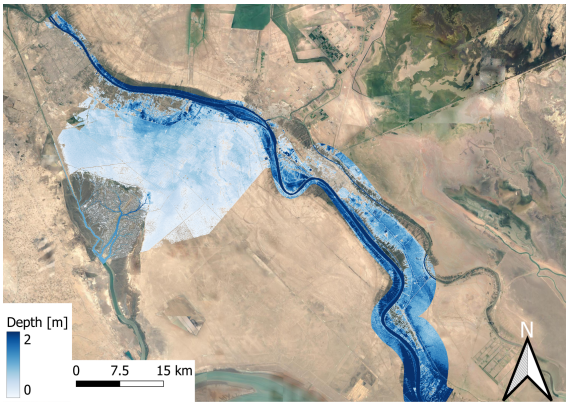

(d) Sc. CC80F, Jul., max.

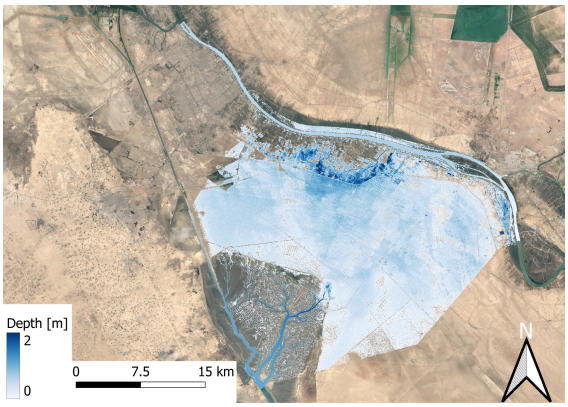

(e) Sc. AC80F, Nov., min.

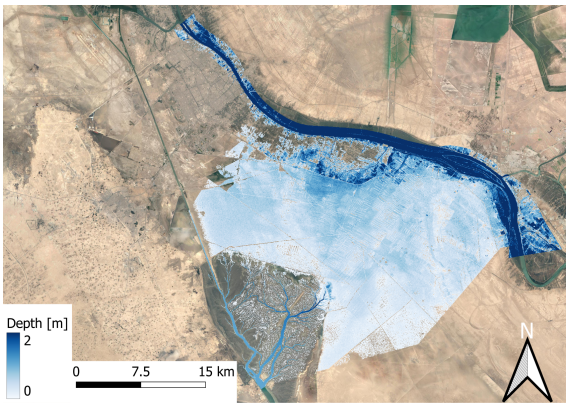

(f) Sc.2, Nov., max.

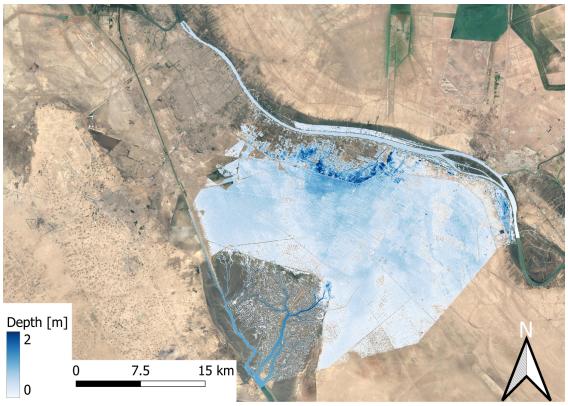

(g) Sc. AC80F, Jul., min.

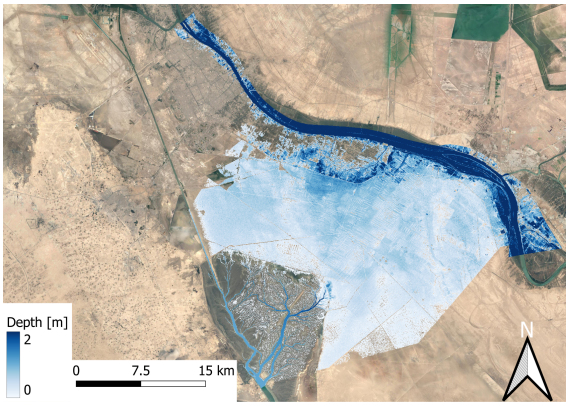

(h) Sc. AC80F, Jul., max.

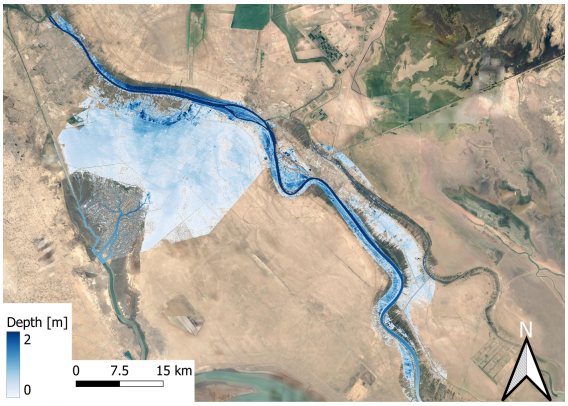

(i) Sc. CC60F, Nov., min.

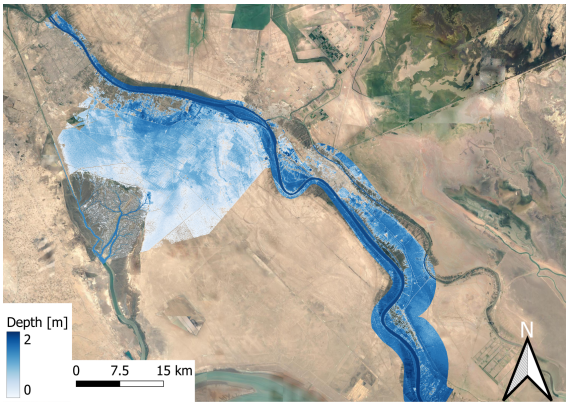

(j) Sc. CC60F, Nov., max.

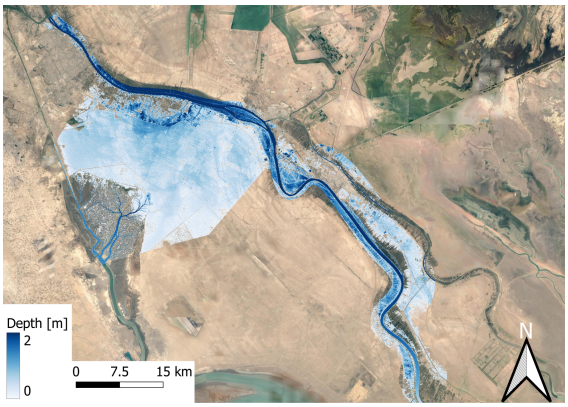

(k) Sc. CC60F, May, min.

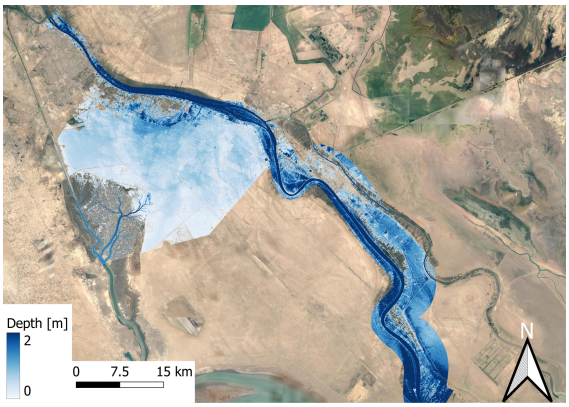

(l) Sc. CC60F, May, max.

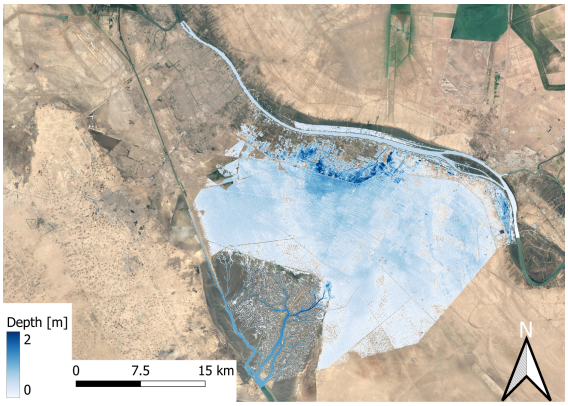

(m) Sc. AC60F, Nov., min.

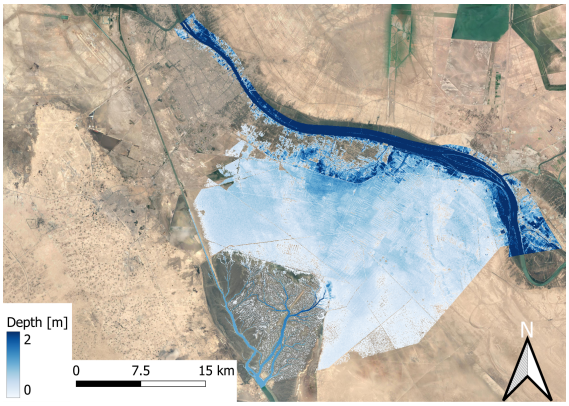

(n) Sc. AC60F, Nov., max.

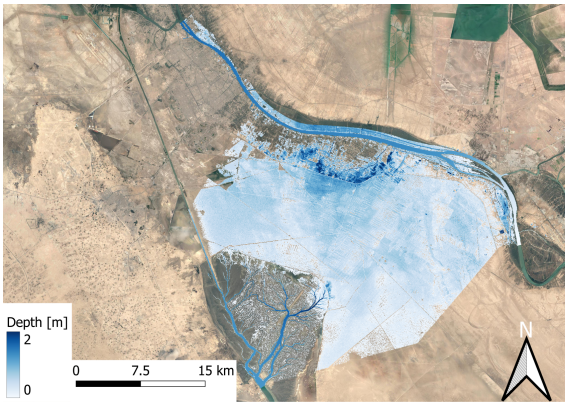

(o) Sc. AC60F, May, min.

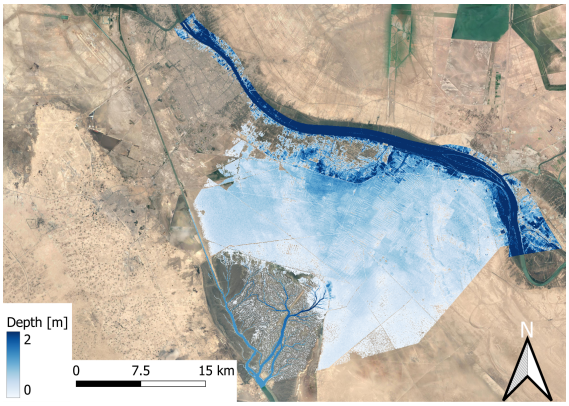

(p) Sc. AC60F, May, max.

Figure 8: Water depth maps for all scenarios showing both the minimum and maximum depth state of the simulation. Be aware that the scale differs depending on the location of the coast.

Scenario	Month	State	Depth	
			Max	Mean
1: CC80F	Nov	Min	4.26	0.50
		Max	4.33	0.55
	Jul	Min	4.25	0.49
		Max	4.32	0.55
2: AC80F	Nov	Min	4.27	0.47
		Max	4.46	0.58
	Jul	Min	4.26	0.47
		Max	4.46	0.58
3: CC60F	Nov	Min	4.25	0.49
		Max	4.32	0.55
	May	Min	4.37	0.58
		Max	4.41	0.61
4: AC60F	Nov	Min	4.26	0.47
		Max	4.46	0.58
	May	Min	4.31	0.50
		Max	4.48	0.62

Table 6: Summary of the depth results of all simulations.

Table 6 shows the maximum and mean depth values achieved for each depth state of each scenario. For clarification, the minimum and maximum depth states, refer to a single point in time in a simulation that either has the overall minimum, or overall maximum water depth generalized over the entire simulated area. However, the maximum and mean depth values, refer to water depth values measured only in the ridge area. Further, the maximum and mean depth values, are measured in both the minimum and maximum depth states. For example, the minimum depth state may have occurred at 12 pm, this would be the point in time when the average water depth is the lowest in the entire simulated area. The maximum water depth in the ridge area measured at the same time, would be referred to as the maximum depth value, during the minimum depth state.

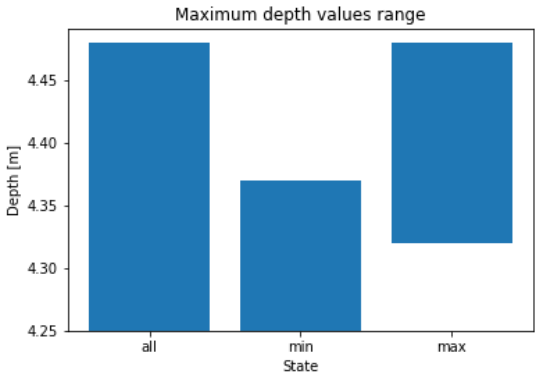

Figure 9: Maximum depth values range across all scenarios for both depth states, then each state separately.

The minimum depth values are the same for each scenario and therefore not displayed in the table. As the ridge area is never entirely covered by water, the minimum depth value is simply the lowest measurable level of water. The maximum depth values vary between 4.25 m and 4.48 m in both the minimum and maximum depth states, while it varies from 4.25 m to 4.37 m in only the minimum states, and from 4.32 m to 4.48 m in only the maximum states (see figure 9). The mean depth values vary form 0.47 m to 0.62 m in every scenario and state. In only the minimum depth states the mean depth values vary from 0.47 m to 0.58 m, and in only the maximum depth states it varies from 0.55 m to 0.62 m (see figure 12).

The figures 10, 11 and 12 were constructed from the results displayed in table 6. Figure 10 compares the maximum and mean depth values, for both depth states, of the wet and dry season of each scenario. Figure 10a shows the maximum depth values of the minimum state for each scenario and season. The values of one scenario are displayed next to each other, such that the two seasons are in direct comparison. The wet season shows higher values for every scenario than the dry season. The zoomed in figure shows the difference in the values more clearly. Figure 10b shows the maximum depth values at the maximum depth state. In scenario

AC80F, the wet and dry season shows the same depth value, however in all other cases, the wet season leads to larger maximum depth values. In figure 10c the mean depth values of the minimum depth state. Scenario AC80F shows the same depth values for both the wet and dry season, all other scenarios show higher depth values in the wet season. Lastly, figure 10d,shows the mean depth values at the maximum depth state. Here, scenario CC80F and AC80F have the same depth values for the two season, while scenarios CC60F and AC60F have higher depth values in the wet season. In all cases, the dry season never shows a higher value. Figure 11 compares the maximum depth values reached between scenarios with varying coastal locations, for the wet and dry period separately. The top figure shows the maximum depth values reached in the wet period. Two scenarios with the same flow data and at the same depth state are displayed next to each other, and in the same color, therefore the only difference between the two is the location of the coast. Scenarios CC80F and CC60F have today's coast, while scenarios AC80F and AC60F have the interpolated coast. The bottom figure shows the same but for the dry period. It can be seen that in almost every case, the scenario with the higher coast has a higher maximum depth value. The only exception is scenario CC60F at the minimum depth state in the wet period. Here scenario CC60F shows a higher value than scenario AC60F. Similarly, figure 12 compares the mean depth range between scenarios with only a change in coastal location for the wet and dry period separately. The left figure shows the mean depth range for the wet period and the right figure shows the values for the dry period. The range is constructed by the mean values during the minimum depth state (lower value) and during the maximum depth state (higher value). Therefore, the variation achieved throughout one day is shown. Two scenarios with only a change in location are placed next to each other and displayed in the same color. It can be seen that in both the wet and dry period the scenarios with the lower coast show much less variation in the mean depth than the scenarios with the higher coast. It can also be seen that the mean depth is generally greater in those scenarios with greater upstream flow (scenarios CC60F and AC60F).

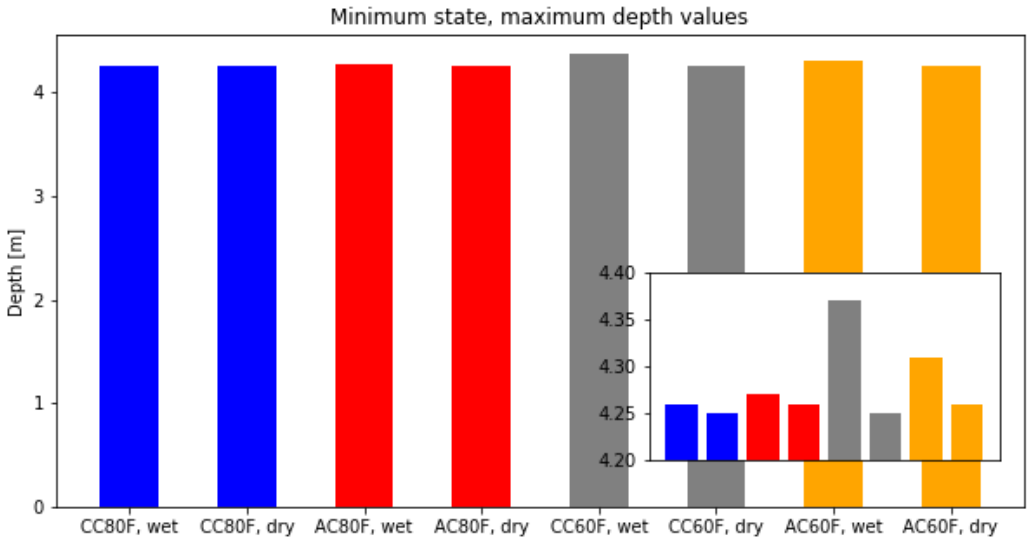

(a) Comparison of the maximum depth values of the minimum depth states for the wet and dry seasons of each scenario.

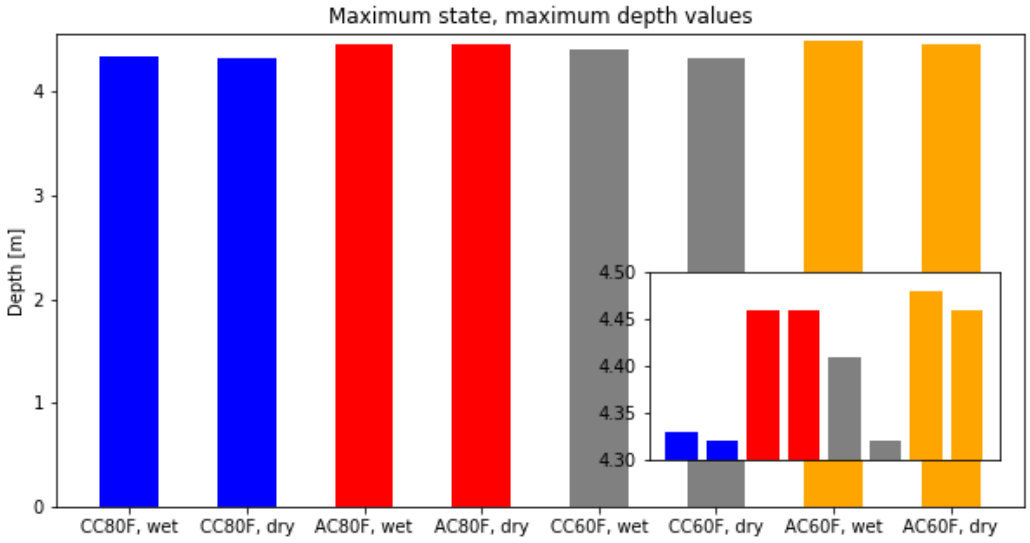

(b) Comparison of the maximum depth values of the maximum depth states for the wet and dry seasons of each scenario.

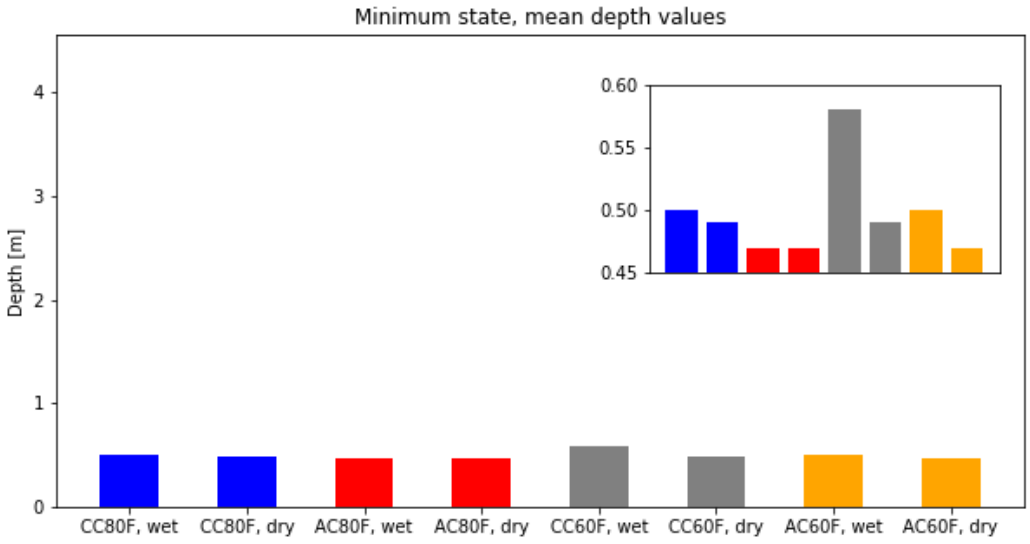

(c) Comparison of the mean depth values of the minimum depth states for the wet and dry seasons of each scenario.

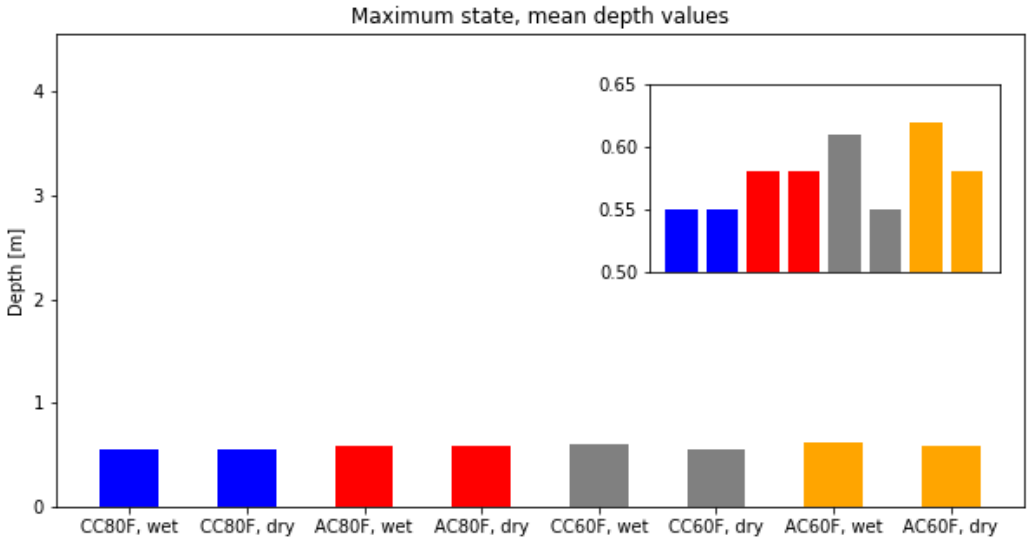

(d) Comparison of the mean depth values of the maximum depth states for the wet and dry seasons of each scenario.

Figure 10: Comparing the maximum and mean depths for each depth state between the wet and dry period. The zoomed in subplot of each plot shows the variation between the values more clearly.

Figure 13 shows a cross-section of the ridge area with the simulated water depth of scenario CC80F in November. The exact location of the cross-section can be seen in the map in figure 14. The top figure shows the water depth in reference to the natural terrain and the lower graph shows only the depth. Above the natural terrain the water surface level is very even and experiences only slight differences in elevation. The magnitude of these differences is quantified in table 6. The depth shown in the lower figure shows greater variation (between 0 m and 2.5 m), which reflects the terrain elevation level in the figure above. The above figure also shows one ridge in the original dimensions as proposed by Nelson (1962) (5 m height, 15 m width). The ridge far extends the elevation of the water surface, with about 2.5 m, while the other half is flooded. This ridge is located in a local minimum in the terrain. If located on a location on the terrain with a higher elevation, the ridge would extend even higher above the water level.

Figure 15 shows the flow from the river into the ridge area for the various scenarios. Negative flow values here refer to reversed flow, so water flowing out of the ridge area back into the river. In each row the results of one scenario for the two seasons are displayed. The left column shows the November simulation results, while the right column shows the summer simulation results. In each scenario the simulation begins with decreasing flow over the lateral structure, until it reaches a local minimum between 3 am and 12 pm. This local minimum is generally reached earlier (by 6 am) in the scenarios with the higher coast (scenario AC80F and AC60F) while it is reached between 9 am and 12 pm is the scenarios with the lower coast (scenarios CC80F and CC60F). Further, the local minima is also lower in the scenarios with the higher coast (about -1000 m^3/s) than in the scenarios with the lower coast (between 0 and -250 m^3/s). Comparing this minima between the seasons of one scenario, it is very similar for all scenarios, except scenario CC60F, where the local minima is much higher (about 500 m^3/s) in the summer season. Again this maxima is reached earlier in the scenarios with the higher coast.

After this local minimum the flow increases again until it reaches a local maxima. This maximum is reached by 12 pm for scenarios with the higher coast, and around 3 pm for scenarios with a lower coast. The reached maximum value is much higher for the scenarios with the higher coast (about 1500 m^3/s vs. $>5000\,m^3/s$). The peaks are reached much more abruptly in the scenarios with the higher coast, while in the scenarios with the lower coast the flow increases more slowly until the peak is reached and decreases more slowly after the peak as well. In scenario AC80F the peak value is very similar in both seasons, however in scenario CC80F, CC60F and AC60F, the wet season has a greater peak value. After the peak the flow decreases again. Only

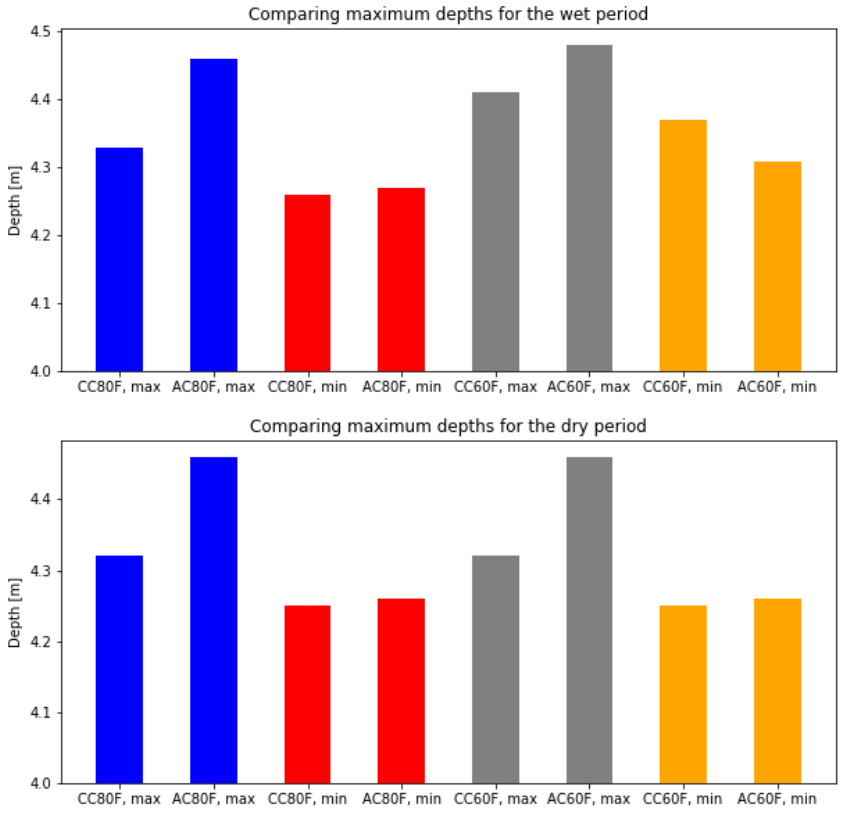

Figure 11: Comparing the maximum depths for each depth state between the scenarios with only a coast location change.

the scenarios with the higher coast reach another minimum value before the end of the simulation. This minimum value is reached around 3 pm and is very similar for both seasons. After this minimum the flow increases again until the end of the simulation.

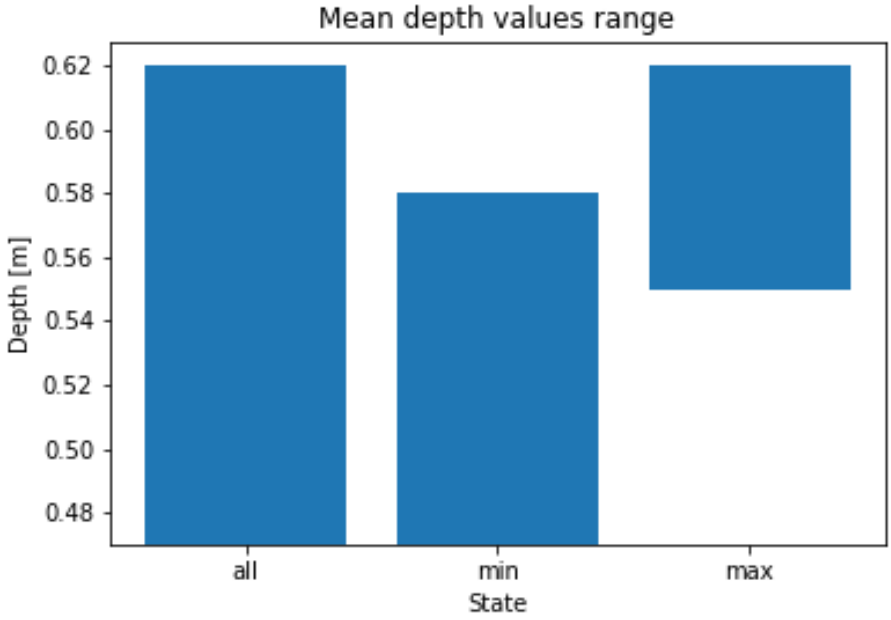

Figure 12: Comparing the mean depth range between scenarios with a higher or lower coast for the wet and dry period.

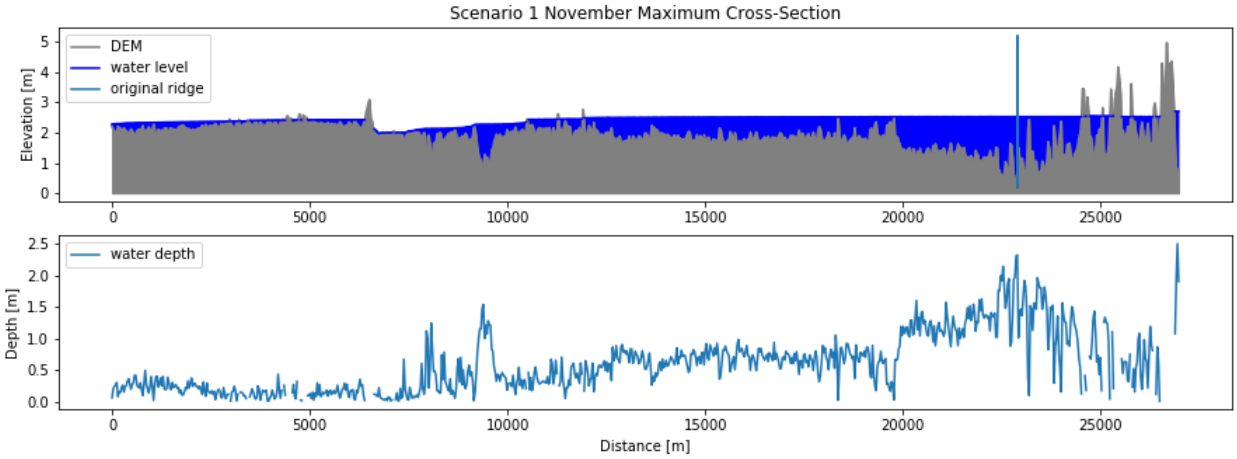

Figure 13: This figure shows the ridge area with the water depth simulated in scenario CC80F run for November. The top figure shows the ridge elevation and the water depth on top of the terrain and the speculated original height of a ridge, while the bottom figure shows only the water depth. See figure 14 for the exact location of the cross-section.

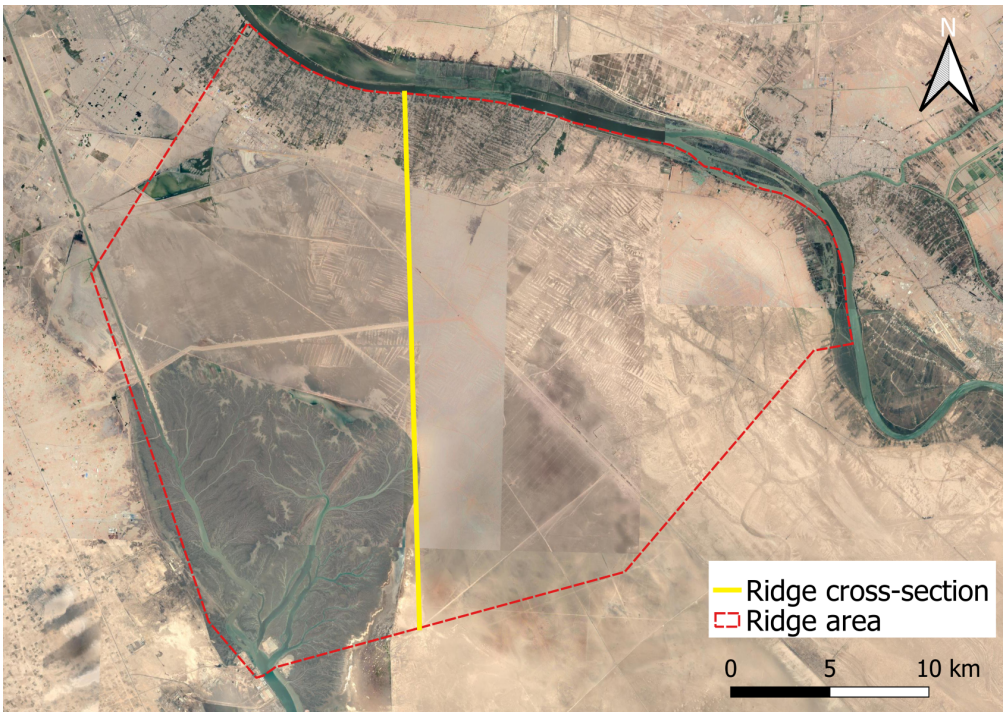

Figure 14: The ridge area and the location of the ridge cross-section shown in figure 13.

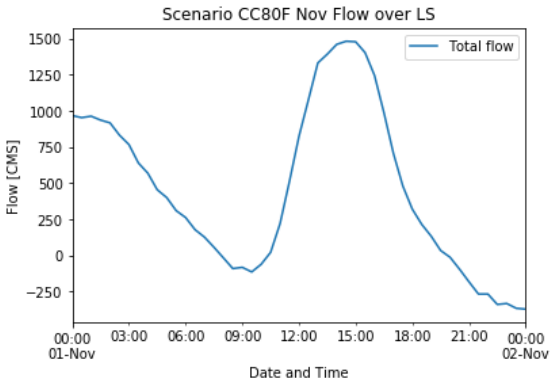

(a) CC80F, Nov.

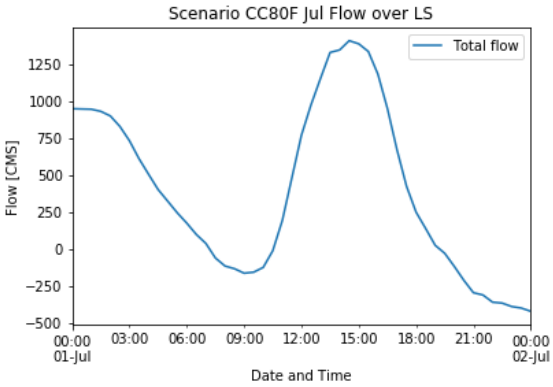

(b) CC80F. Jul.

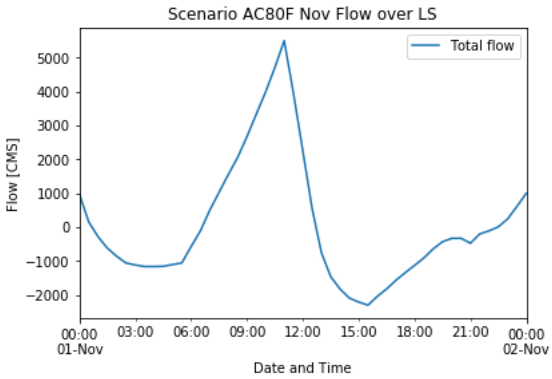

(c) AC80F, Nov.

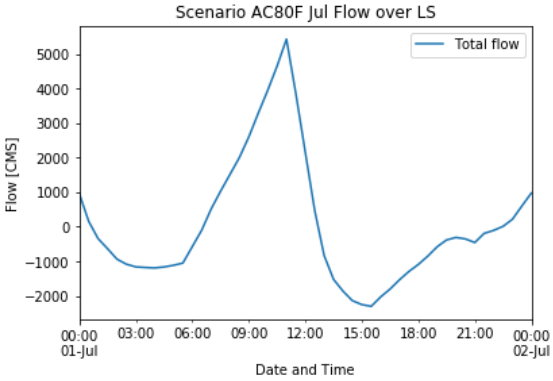

(d) AC80F, Jul.

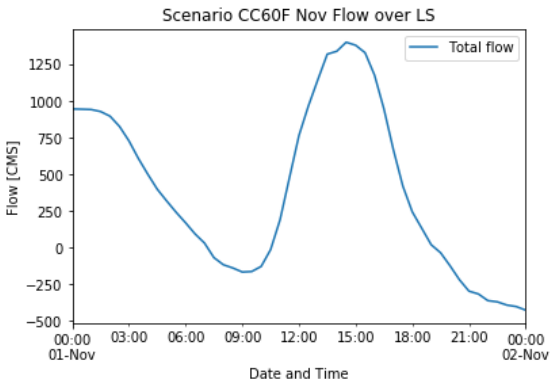

(e) CC60F, Nov.

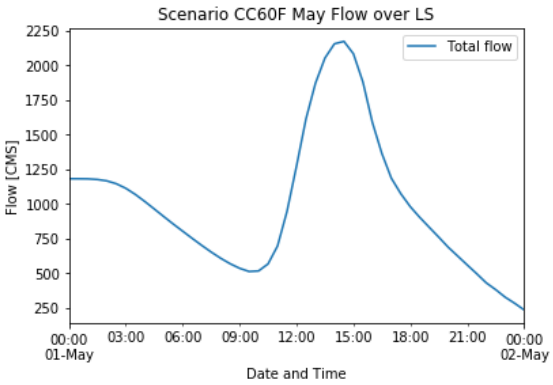

(f) CC60F, May

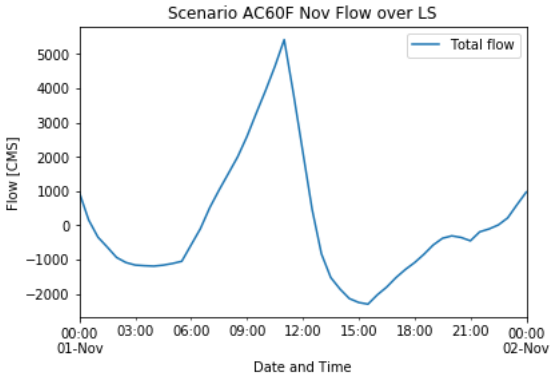

(g) AC60F, Nov.

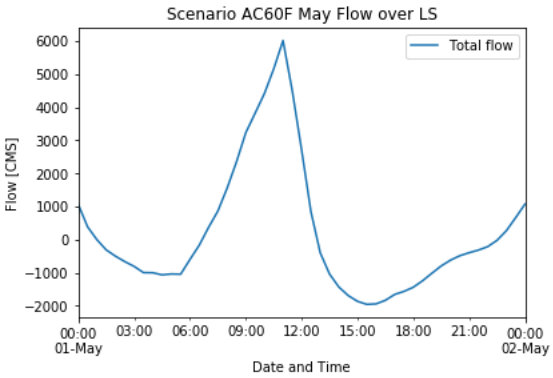

(h) AC60F, May

Figure 15: Flow from the river into the ridge area for scenarios 1-4.

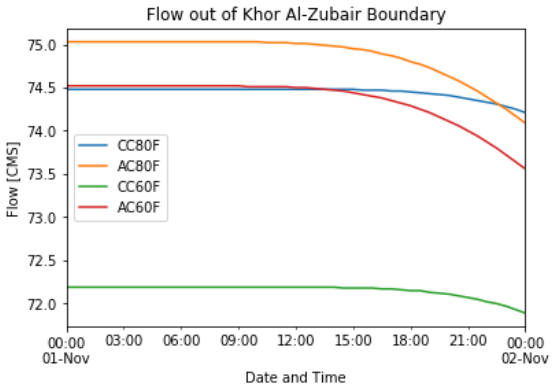

(a) Boundary: Khor Al-Zubair, Nov.

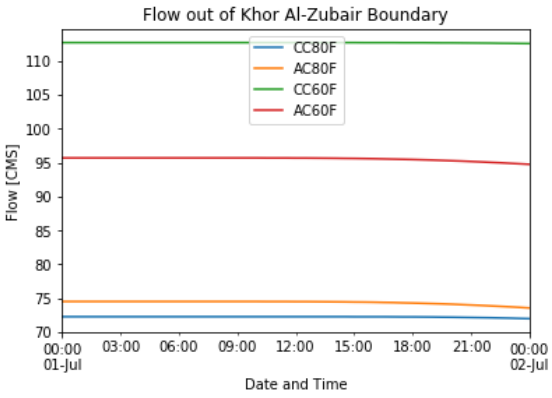

(b) Boundary: Khor Al-Zubair, Jul. and May

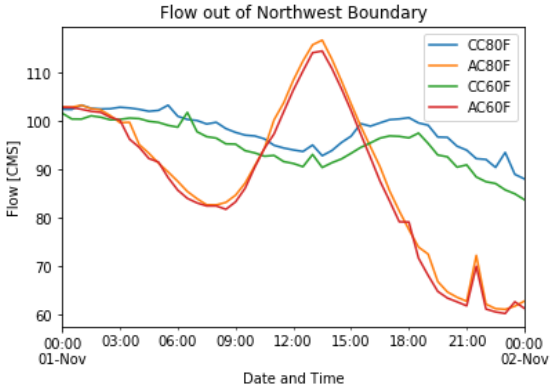

(c) Boundary: North West, Nov.

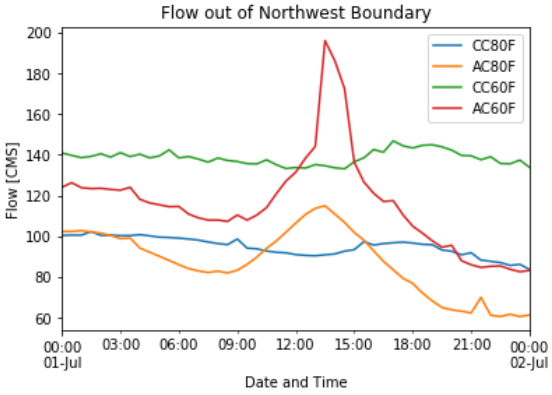

(d) Boundary: North West, Jul. and May

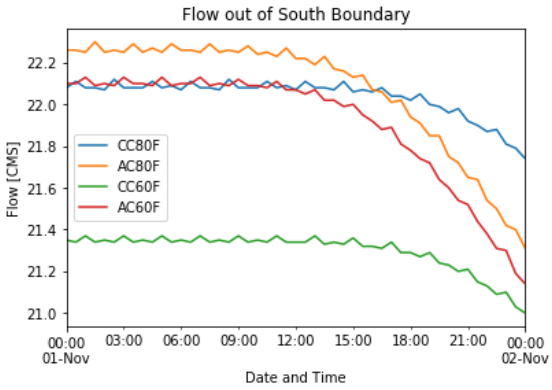

(e) Boundary: South, Nov.

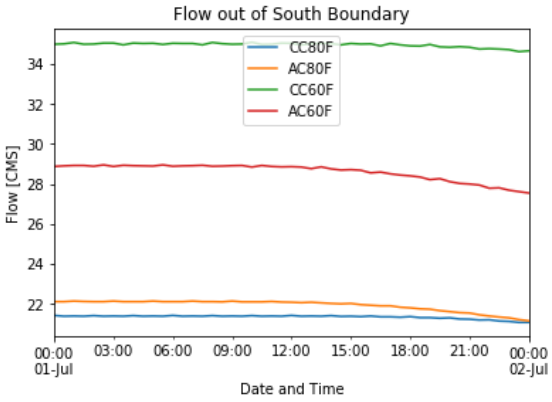

(f) Boundary: South, Jul. and May

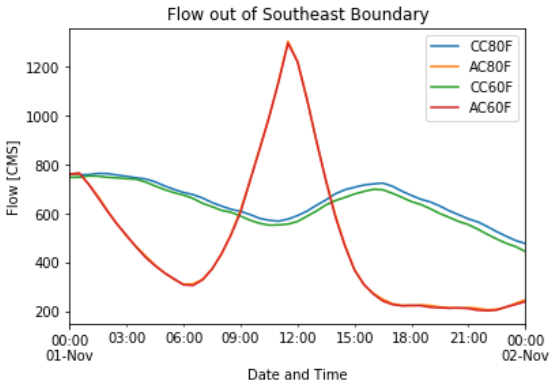

(g) Boundary: South East, Nov.

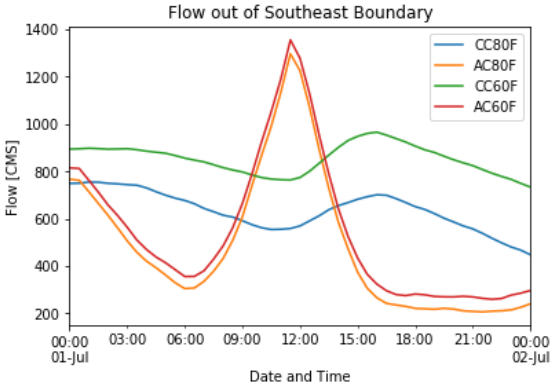

(h) Boundary: South East, Jul. and May

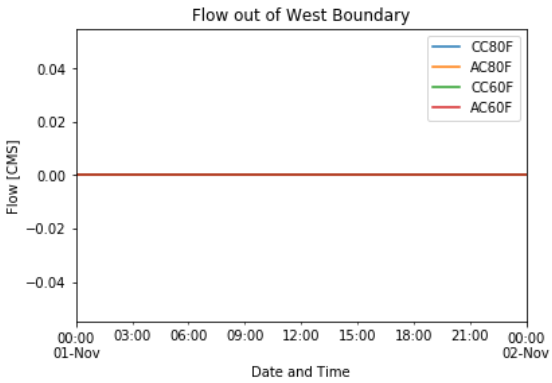

(i) Boundary: West, Nov.

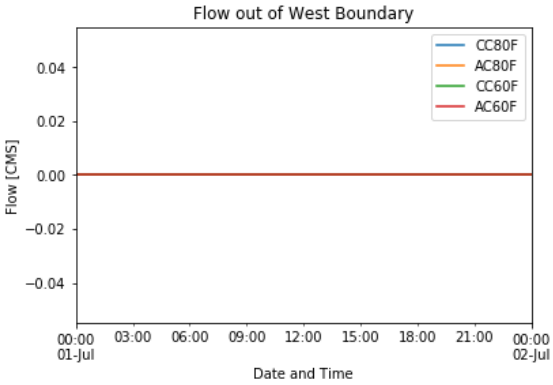

(j) Boundary: West, Jul. and May

Figure 16: Flow from the ridge area outwards over the various boundaries, for scenarios 1-4. See figure 3 for a map with the locations of the boundaries.

Figure 16 shows the flow out of the ridge area over the various boundaries for each scenario, for the two seasons separately. It is important to remember that although the x-axis says July for the summer simulations, Scenario CC60F and AC60F actually take place in May. This figure is explained in more detail in the discussion in section 4.1.1.

3.2 Sensitivity Analysis

Table 7: Comparison of depth in the ridge area between scenario CC60F and the sensitivity analysis with changing river cross-section areas and the sensitivity analysis with an elevated lateral structure (LS) with one inlet.

Month	State	Depth	Sc. 3	Increased XS's		Decreased XS's		Elevated LS	
				abs.	rel.	abs.	rel.	abs.	rel.
November	Max	Max	4.32	4.33	+0.1%	4.62	+7%	4.02	-7%
		Mean	0.55	0.55	+0.3%	0.51	-7%	0.40	-27%
	Min	Max	4.25	4.25	-0.1%	4.18	-1%	4.02	-6%
		Mean	0.49	0.48	-2%	0.46	-6%	0.40	-20%
May	Max	Max	4.41	4.39	-0.4%	5.03	+14%	4.08	-7%
		Mean	0.61	0.60	-1%	0.76	+26%	0.43	-29%
	Min	Max	4.37	4.35	-0.6%	4.60	+5%	4.08	-7%
		Mean	0.58	0.56	-4%	0.71	+22%	0.43	-26%

Table 8: Comparison of depth in the ridge area between scenario CC60F and the sensitivity analysis with 2 inlets in a heightened lateral structure (LS), between scenario CC60F and increased, as well as decreased, boundary conditions around the ridge area, and between scenario CC60F and the sensitivity analysis where the river can flood along its entire length.

Month	State	Depth	Sc. 3	LS 2 inlets		Increased BC		Decreased BC		Flooded River	
				abs.	rel.	abs.	rel.	abs.	rel.	abs.	rel.
November	Max	Max	4.32	4.17	-3%	4.32	0.0%	4.33	+0.1%	4.29	-0.8%
		Mean	0.55	0.48	-12%	0.54	-0.3%	0.55	+0.4%	0.37	-32%
	Min	Max	4.25	4.17	-2%	4.25	0.0%	4.25	0.0%	4.23	-0.4%
		Mean	0.49	0.46	-6%	0.49	-0.4%	0.49	+0.5%	0.34	-31%
May	Max	Max	4.41	4.41	0.0%	4.40	-0.1%	4.41	0.0%	4.37	-0.9%
		Mean	0.61	0.61	0.0%	0.60	-0.5%	0.61	0.0%	0.44	-28%
	Min	Max	4.37	4.37	0.0%	4.37	-0.1%	4.37	0.0%	4.28	-2%
		Mean	0.58	0.58	0.0%	0.58	-0.5%	0.58	0.0%	0.40	-31%

Tables 7 and 8 compare the water depth in the ridge area, when any of the sensitivity analysis parameters are altered, with the results of scenario CC60F. The column 'Increased XS's' refer to the sensitivity analysis in which the river cross-sections were enlarged by 25%, while 'Decreased XS's' refer to the sensitivity analysis in which the river cross-sections were decreased by 25%. The 'Elevated LS' column refers to the sensitivity analysis in which the lateral structure was elevated to 5 m height and was given one inlet. 'LS 2 inlets' refers to the sensitivity analysis in which the lateral structure was elevated and given two inlets. The columns 'Increased BC' and 'Decreased BC' refer to the sensitivity analysis simulations in which the boundary conditions of the boundaries of the 2D flow area were increased, then decreased by 20%, respectively. Finally, the column 'Flooded River' refers to the sensitivity analysis in which the river could flood along its entire length, instead of only at the ridge area location.

4 Discussion

4.1 Discussion of the Results

4.1.1 Scenarios

To begin, the figures and tables in section 3 were interpreted individually.

Figure 8 Analysing figure 8, it is firstly important to note than in every scenario, the ridge area is almost entirely flooded. In both the wet and the dry season, there is flooding between the ridges, while the ridges extend above the water level and stay consistently dry. Secondly, the depth distribution is very similar in each figure: the greatest depths ($\geq 2\,\mathrm{m}$) are achieved in the northern section of the ridge area and gradually become shallower towards the south, east and west ($< 1\,\mathrm{m}$). Lastly, for each scenario slight differences in the depth distribution between the minimum and maximum state can be seen, although the variation in the blue color intensity is not strong enough to be able to point out specific differences with the bare eye. This means that the area is so large that an increase in flow values or a change in the coastal location does not change the depth very much. The pattern of depth distribution does not seem to change.

Table 6 Table 6 confirms the observations made above that although differences can be seen between the scenarios the variation is not very large. Similarly, differences can be seen between the minimum and maximum depth states, but again they are not very large. The depths increase when there is greater flow (for scenarios CC80F and AC80F, depths are greater in November than in July, for scenarios CC60F and AC60F, depths are greater in May than November) (see figure 10) and maximum depths increase with the higher coast (maximum depths are greater in scenario AC80F than scenario CC80F and in scenario AC60F than scenario CC60F) with the only exception of scenario AC60F, May in the minimum depth state, which shows a lower value than scenario CC60F, May in the minimum depth state (see figure 11). When the coast is higher, then the depth varies more, so the maximum depths are greater, as discussed above, and the mean of the minimum state is lower and the mean of the maximum state is greater (see figure 12).
The similarity in depth between the scenarios may be caused by the terrain determining the maximum possible depth. In this case the depth would stay constant even if the inflow values change, as long as the inflow can be balanced by the outflow and a minimum threshold is crossed such that the system can be filled. Slight variations in depth could indicate that not all pockets in the terrain were yet filled, or that locally the inflow is not balanced by the outflow.

Figure 15 In each of the sub-figures in figure 15, the tidal effect on the flow can be clearly seen. Further, there is a time delay in maximum flow into the ridge area in those scenarios with the lower coast. A lower coast also decreases the flow amplitude and widens the wavelength of the flood wave. When comparing the graphs of scenarios with the same model geometry but differing flow data (scenario CC80F vs. scenario CC60F, and scenario AC80F vs. scenario AC60F) it can also be seen that higher upstream flow leads to greater flow into the ridge area. In scenario CC60F May, the combination of the lower coast and higher upstream flow causes water to constantly flow from the river into the ridge area and not to reverse. When taking another look at table 6 and comparing the mean and max depths of scenarios CC80F and CC60F in their respective wet season, it can be seen that the depth has increased by 6 cm - 12 cm in scenario CC60F. This shows that, although, in this scenario and season the ridge experiences constant inflow of river water, the water depth in the ridge area does not increase by more than 12 cm. Therefore, increased flow into the ridge area does increase the water depth, however it does not cause any extreme variation. This also shows that the flow into the system is balanced well by the flow out of the system and therefore regulates the water depth that can be achieved. This confirms the general findings listed above for table 6.

Figure 16 In figure 16, some model instability can be detected, especially in sub-figures 16c, 16d, 16e and 16f. The instability can be detected in the light zigzagging appearance of the flow curves. To decrease model instability smaller time steps and therefore larger simulation run-time would be required. However, since the fluctuations caused by model instability are relatively small, and the general trends and magnitude of flow can still be clearly detected, this degree of instability can be accepted for the purpose of this study.

The flow out of the Khor al-Zubair, South and West boundaries, which can be seen in figure 16, show a similar pattern for all the scenarios, with differing absolute values, except for the west boundary, which experiences 0 flow for all scenarios and seasons. The reason the West boundary experiences no flow is due to the fact that the Khor al-Zubair flows before the West boundary draining all of the water. The Northwest and Southeast boundaries experience different flow patterns based on the scenario.
Figures 16a, 16b, 16e, and 16f show a very similar flow pattern: stable flow values at first, which later in the day begin to exponentially decrease. The simulations for November show the same order of scenarios ordered by highest to lowest flow values and the summer simulations also show the same order. In November this order is scenario AC80F, AC60F, CC80F, then CC60F.

- Scenario AC80F has a higher coast than scenarios CC80F and CC60F and greater flow values than scenario CC60F and AC60F.
- Scenario AC60F has a higher coast than scenario CC80F and CC60F but lower flow than scenarios CC80F and AC80F.
- Scenario CC80F has higher flow values than scenario CC60F and AC60F, but a lower coast than scenario AC80F and AC60F.
- Finally, scenario CC60F has the lower flow values and the lower coast.

This shows that a higher coast and higher flow values lead to greater flow out of the boundaries, where a higher coast has a stronger effect than the increase in flow between the scenarios in the month of November. Further, it is interesting that scenarios AC80F and AC60F show greater variation in the flow over the boundary, while scenarios CC80F and CC60F are more stable. This confirms the observations from table 6, which showed that a higher coast led to greater flow variations than the lower coast.
In the summer months the order of the scenarios ordered from highest to lowest flow is scenario CC60F, AC60F, AC80F, then CC80F, showing that greater upstream flow leads to greater flow out of the boundary, however the effect of the coast location differs. In the case of scenario CC60F vs. AC60F, the lower coast leads to greater flow out of the boundary, while in the case of scenario CC80F vs. AC80F, the higher coast leads to greater flow out of the boundary.

Figures 16c, 16d, 16g and 16h also show very similar patterns, with both the November and summer simulations showing the same order. In November, scenarios AC80F and AC60F are very similar, although in the case of the Northwest boundary, scenario AC80F experiences a little more flow than scenario AC60F. Scenarios CC80F and CC60F show the same flow pattern, with scenario CC80F having slightly higher flow values. The first observation to be made here is the different flow patterns between the scenarios AC80F and AC60F, and CC80F and CC60F. The scenarios with the same coast location show similar flow patterns, where the scenarios with the higher coast show larger flow variations and an earlier peak in flow. This observation again confirms the observations made for table 6. Secondly, the scenario with higher upstream flow values shows greater flow out of the boundary, except for the case of scenarios AC80F and AC60F in figure 16g, which show the same flow values. In the summer simulation the coast location has the same effect on the flow pattern, however the order is reversed between the scenarios with the same coast location, as scenarios CC60F and AC60F have higher flow values than scenarios CC80F and AC80F in this season.

The similarities between the flow patterns of the boundaries Northwest and Southeast, and Khor al-Zubair and South can be explained by their location which can be seen in figure 3. The Northwest and Southeast boundaries are connected to the river, meaning that some of the flow through the river goes over these boundaries and therefore affects the pattern of flow over these boundaries. Boundaries Khor al-Zubair and South on the other hand are distant from the river and therefore not directly affected by the flow through the river itself.

Generally, what can be concluded from the results shown in figures 15 and 16, is that the water level in the ridge system is replenished daily, all year round. The locations, times and magnitude of in- as well as outflow can be deducted from the same figures. Therefore, the maintenance of a marshland does not depend on water inflow in the wet season, to last through a dry season with no replenishment of the water. Further, the magnitude of in- and outflow of water, shows that the water in the ridge system is not entirely still, but does experience some renewal.

4.1.2 Sensitivity Analysis

River Cross-Sections The change in water depth, shown in table 7, is very small when the cross-sections are increased, under 1% in all but 3 cases, up to 4% in all cases. However, when they are decreased the change in water depth is up to 26%, and above 5% in more than half of the depth states. Decreasing the cross-sections causes the mean water depth to decrease by 6% and 7% in November, while it increases by 22% to 26% in May. The maximum depth increased by 5% to 14% in all cases, except for the minimum depth state in November, when the maximum depth decreased by 1%. The maximum depth of the maximum depth state in May is the only simulated depth which would have caused flooding of the ridges. The difference between November and May were likely caused by the difference in upstream flow, which is much greater in May than in November. It is unclear what may have caused the decrease in maximum depth in the minimum depth state of November. Perhaps the answer lies in the pattern of in- and outflow, however, this pattern was not analysed in the sensitivity analysis of this study.

Flow from river to ridge area The values under 'Elevated LS' are generally lower than the values in scenario CC60F, with no depth scenario increasing by more than 0.2% and decreases reaching up to 29%. Especially the mean depths decrease drastically (-20% to -29%), while the maximum depths decrease by 5% to 7%. A further interesting observation is that there is no depth variation throughout the day and very minimal seasonal variation (max. 6 cm).
However, when a second inlet is added to the lateral structure the depth changes are much less, with those in May not changing at all and those in November decreasing by max. 12%. There is also more variation visible throughout the day and seasonally in this scenario. Although the daily and seasonal change is still relatively small, up to only 12 cm.

Boundary Conditions Changing the boundary conditions of the ridge areas had very little affect on the depth in the ridge area, less than 1% in all cases and for May with decreased boundary conditions it had no effect. However, it is still interesting to note that when the boundary conditions are increased the depth tends to decrease, while when the boundary conditions are decreased, the depth tends to increase.

River flooding The effect of enabling the river to flood varies greatly depending on which characteristic is observed, as can be seen in table 8. The maximum depth decreases by less than 1% in all but the minimum state in May, which decreases by 2%. However, large effects can be seen on the mean depth for every depth state. The mean depth is decreased by 28% to 32%, in absolute numbers this translates into a decrease of 15 cm to 18 cm. The mean depth now varies from 0.34 m to 0.44 m.

4.2 Answering the Research Questions

To answer the research questions, the sub-questions will be discussed first to conclude with a final discussion on the main research question.

Where does flooding take place in the ridge system? The water depth was not spread equally throughout the ridge area, dry areas occurred mainly in the north of the ridge area and in the Khor al-Zubair delta. Smaller dry areas also occurred along the river bed and in the south of the ridge area.

When is the ridge system flooded and how is this affected by seasonal upstream flow changes and daily tidal variations? Flooding occurred year-round, during the wet and dry periods, and all day long, during high and low tide. Tidal variations caused changes in water depth throughout the day, however the extent of these variations was largely affected by the distance of the ridge area to the coast. In either case, daily variations did not exceed 20 cm. Seasonal variations were caused by the differing upstream flow in the wet and dry seasons and lead to a maximum depth variation of 12 cm.

How deep is the water when the landscape is flooded and how does the depth vary throughout the landscape? The deepest depths occurred in the north of the ridge area with shallower depths in all directions from there. The average depth varied from 0.47 m to 0.62 m, and the maximum depth from 4.25 m to 4.48 m in all the simulated scenarios.

What does the flow pattern into and out of the ridge system look like? The flow into and out of the ridge system is strongly affected by the tidal pattern, where the location of the coast determines the extent of flow variation throughout the day. A higher coast leads to larger variation than a lower coast.
Water flows into and out of the ridge area both in the wet and dry season. This shows that the water is replenished throughout the year and does not depend on a wet season for replenishment while it is depleted in the dry season.

In how far does the ridge system resemble a marshy area with elevated fields? As the ridges have been hypothesized to have been 5 m tall (Nelson, 1962) when the irrigation system was utilized, the ridges would never have been flooded. In the main scenarios the maximum depth reached was 4.48 m, while the mean depth ranged from 0.47 m to 0.62 m, therefore a ridge height of about 70 cm would have sufficed in most of the ridge area, while some local ridges may have needed to be up to 4.5 m to prevent them from flooding. View figure 13 to see a cross-section of the ridge area with the water depth from scenario CC80F run for November compared to the speculated original height of the ridges.
As data availability was very limited, many of the input parameters were based on approximations or averages. The first of these were the river-cross sections, therefore the effect of differing river-cross sections was analysed. The results show that larger cross-sections barely affect the water depth in the ridge area, while smaller cross-sections significantly increase the depth in the ridge area, especially during the wet period. Decreasing the cross-sections, without changing the flow leads to significantly more flooding, which increases the water depth in the ridge area. However, why the depth barely changes when the cross-sections are increased is not clear. Increasing the cross-sections should lead to decreased flooding, which would be expected to decrease the depth in the ridge area. The reaction of the water depth in the ridge area to a change in river cross-section area, therefore requires further exploration for a more detailed understanding of the system.
A further important factor is how the flow from the river into the ridge area may have been managed, if at all. If the flow from the river into the ridge area was managed with a singular inlet (of approximately 75 m width), rather than letting the water freely flood the area, the water depth would have been significantly decreased. However, if more than one inlet (accumulated width of approximately 150 m) was used the water depth would not have been affected at all during the wet period, while during the dry period especially the mean depth would have been affected and decreased by up to 12%.
The final approximated parameters were the boundary conditions of the 2D flow area. However, neither increasing nor decreasing them by 20% caused significant changes (less than 1% in all cases) in the simulated water depths.
Lastly, the model geometry was altered such that the river could flood along its entire length, rather than just in the location of the ridge area. This had the largest effect on the water depth in the ridge area, decreasing the mean depth up to 32%, however, even in this scenario, the mean depth did not decrease lower than 0.34 m, maintaining the constant flooding of the ridge area.
It can be concluded that the ridge area was easily flooded, except for few small areas that stayed dry, while the ridges would stay completely dry. Further, it should be noted that the only possibility of the areas between the ridges having been used for agriculture, would require plants that grow under constant flooding. Alternatively, the flooded area could also have been used for pisciculture. These two options require further exploration though, their potential success has not been evaluated within this study.

4.3 Limitations

As has already been repeatedly stated, data availability was very poor and all data that was used was based on relatively modern measurements (1948 and later). Limitations were therefore met in both the geometrical and hydrological representation of the original system.
The geometrical limitations were set by the digital elevation map, the location of the river and the location

of the coast. The effect of a varying coast location was explored in the sensitivity analysis, meaning that the effects of this could be quantified. However, no conclusions can be made about where the coast might have actually been and therefore which scenario might be more realistic.
Secondly, the digital elevation map was measured between 2011 and 2015, therefore the ridges are largely eroded, former canals are no longer present and other unforeseen changes may have taken place. The inclusion of an elevated lateral structure in the sensitivity analysis explores the effect of a natural or built levee, however, again no conclusions can be made on the likelihood of such a levee existing. Further information on the former terrain is very limited. The assumption that the ridges may have been 5 m high originally stems from one source only, and the origin of this idea is not made clear in this source (Nelson, 1962). Considering that the average water depth reaches a maximum of 0.62 m (in the four scenarios), capillary rise may not have sufficed to provide crops on the ridges with water, therefore, creating a cause to doubt the speculated original dimensions of the ridges.
Finally, the river itself will likely have flown along a different path than it does today, however, as no data on the former path of the river was available, this change could not be explored in the simulations. Consequently, the river bathymetry would also likely have largely differed from the measurements today, the effect of varying river cross-section size was explored in the sensitivity analysis, but the effects of local changes in the river bathymetry could not be explored due to a lack of data.

Changes in the river flow were explored in the four scenarios and the sensitivity analysis, still it is important to keep in mind that no data was available to set a realistic range in river flow variation. Another limitation in the upstream flow data, is that it has a relatively low resolution, meaning that the effect of daily flow variations, or even extraordinary events, such as floods or droughts, could not be explored. Changes in the stage hydrograph were also not explored, although it is possible that it may have differed during the time period of interest.
Lastly, it was chosen to run the scenarios for November rather than October, which is the driest month in the data shown in table 3. This was done because the barley growth season starts in November, therefore it was of interest if water would be available during the growth season of the crops. However, as a consequence, what the depth distribution looked like in the ridge area in the driest month of the year was not explored. Nevertheless, it can be expected that the variation from November would be very small, as the difference in flow values is only 57 m^3/s and the difference between the simulated months November and May is 2,016 m^3/s and resulted in a maximum variation of 12 cm for the maximum depth and 9 cm for the mean depth.

The model was also limited by the fact that it did not include evaporation or infiltration losses. As mentioned in section 2.4 evaporation is very high in Iraq due to the high temperatures, therefore it may significantly impact the depth in the ridge area. Soil infiltration was not further discussed within this study, the impacts of which would need to be estimated to gauge its impact on the water depth in the ridge area.

5 Conclusions and Recommendations

5.1 Conclusions

This study explored the possibility of the landscape of the ridge area in ancient Basrah resembling a marshy area, such that the ridges may have been used as elevated fields. To explore the possible function of the ridge system a hydraulic model was set up in HEC-RAS. To set up this model modern data had to be utilized, as data of the period of interest was not available. This data included a digital elevation map, river cross-sections, river flow, stage measurements and information derived from the digital elevation map, such as the coast location and the energy slope along the boundaries of the hydraulic model.
Four scenarios were set up, which differed in flow in the Shatt Al-Arab and the coastal location, further multiple sensitivity analyses were run to quantify the impact of estimated boundary conditions. The results showed that it is highly likely that the ridges resembled elevated fields, as flooding occurred during both the wet and dry season and all day long (at high and low tide) in the ridge system. The average water depth varied from about 0.3 m to 0.6 m and the maximum water depth stayed below 5 m (except for one case in a sensitivity analysis run), which would mean the ridges were not flooded, as they are said to have been 5 m tall. Flow into and out of the ridge system occurred all day long, during both the wet and dry season, describing the functionality of the system as not being dependent on high inflow in the wet season and drying during the dry period, but relatively stable water availability all year round. It also shows that the water was refreshed continuously, possibly maintaining a certain level of water quality.
Further, seven sensitivity analysis were run, to test the sensitivity of the model towards a change in the river cross-section size, the style of flow from the river into the ridge area (floodplain vs. controlled), varying slope of the terrain at the boundaries of the ridge area and flooding of the river along its entire length versus just in the location of the ridges. The results showed that the system was most affected by decreasing the river cross-sections, changing the flow style from the river to the ridge area, and by allowing the river to flood along its entire length. These changes caused the depth in the ridge to change within a maximum range of -31% to +26%. In the case of increasing the cross-sections or changing the boundary conditions along the edges of the ridge system, the maximum variation in depth was -4% to +0.5%.
Research on the functionality of the ancient irrigation system has so far mainly assumed that the ridges were a product of removing salinized topsoil of the basins in between the ridges, which was originally proposed by Nelson (1962). The results of this study show that the hypothesis of the ridges having been used as elevated fields, while the rest of the area was marshy, should be seen as plausible and explored in further research.

5.2 Recommendations

Firstly, to confirm or deny the results of this study, the boundary conditions during the time of interest would need to be studied and compared to the boundary conditions utilized in this study. If the boundary conditions of the time of interest fall within the range explored in this study, it would confirm the findings, while variations from the range would require further study of the flooding of the ridge area. Boundary conditions that were found to have especially great impacts on the level of flooding and should therefore receive ample attention in further research, are

- the amount of upstream flow in the Shatt Al-Arab,
- the location of the coast,
- the river cross-sections, especially if they may have been smaller than they are today,
- a natural or constructed levee along the Shatt Al-Arab and the number and width of accompanying water inlets to the ridge system,
- and finally, the flooding of the river downstream of the ridge area, however this would depend on the above listed parameters, such as the coast location, the river cross-sections and the presence of a natural or built levee system on the river banks.

To further explore the possibility of the ridges having been used as elevated fields, two more aspects would need to be analysed. Firstly, it has been found that the salt content of the ridges is double the salt content of

the basins in between the ridges (15 mmhos\cm in the basins vs. 30 mmhos\cm in the ridges) and therefore no vegetation can grow on the ridges (Kennedy, 2011; Nelson, 1962). The hypothesis that the ridges are discarded salty topsoil is mainly based on this fact. Therefore, the possibility of the salt content accumulating naturally through capillary rise and evaporation of water needs to be explored. Quantification of the number of years it would take for the salinity to increase from the value found in the basins to the values found in the ridges through the above mentioned process, would show when the ridges would have attained a salinity level too great for agricultural production. In this analysis the balance of water evaporation and inherent salinity increase of the water in the ridge system, with the replenishment of the water should also be considered.
The second aspect that needs to be explored is the success of crop growth on the ridges. This could be done in a similar manner as this study, through the setup of an exploratory crop growth model with varying scenarios, given the water levels found in this study. This could also be used to identify a realistic range for the height of the ridges, under the assumption that they were used as elevated fields. Creating different crop growth scenarios with varying ridge heights, would allow the determination of a ridge height at which the capillary rise would suffice to provide the root zone of the crops with sufficient water.
Similarly, it could be investigated how crops could have been successfully cultivated. If the crops require a certain root depth to reach the water, it would be of interest to find out how the crops would successfully reach that minimum root depth, before which they would require an alternative means to water. Finding that local crops, such as barley, could have been successfully cultivated on the ridges, would further support the hypothesis of the ridges serving the function of elevated fields.

References

Al-Asadi, S., Abdullah, S., & Al-Mahmood, H. (2015). Estimation of minimum amount of the net discharge in the shatt al- arab river (south of iraq). *Journal of Adab Al-Basrah*, *2*, 285—314. (In Arabic)

Al-Asadi, S. A., & Alhello, A. A. (2019). General assessment of shatt al-arab river, iraq. *International Journal of Water*, *13*(4), 360–375.

Ali Ghorbani, M., Kazempour, R., Chau, K.-W., Shamshirband, S., & Taherei Ghazvinei, P. (2018). Forecasting pan evaporation with an integrated artificial neural network quantum-behaved particle swarm optimization model: a case study in talesh, northern iran. *Engineering Applications of Computational Fluid Mechanics*, *12*(1), 724–737.

Al-Mahdi, A., & Salman, H. (1997). Some hydrological characteristics of the shatt al-arab river, south of iraq. *Marina Mesopotamica*, *12*(1), 63—74.

Al-Taei, S. A., Alfartusi, A. J., & Abdulhussein, I. A. (2019). Determination of hydrodynamic resistance coefficient (manning's coefficient) in shatt al arab river, southern of iraq-basrah. *Journal of Engineering and Sustainable Development*, *23*(03).

Brandimarte, L., Popescu, I., & Neamah, N. K. (2015). Analysis of fresh-saline water interface at the shatt al-arab estuary. *International Journal of River Basin Management*, *13*(1), 17–25.

Bremer, N. (2013). *Water law and cooperation in the euphrates-tigris region.* Brill — Nijhoff.

Campbell, G. (2016). East africa in the early indian ocean world slave trade: The zanj revolt reconsidered. In *Early exchange between africa and the wider indian ocean world* (pp. 275–303). Springer.

Comptour, M., Caillon, S., Rodrigues, L., & McKey, D. (2018). Wetland raised-field agriculture and its contribution to sustainability: Ethnoecology of a present-day african system and questions about precolumbian systems in the american tropics. *Sustainability*, *10*(9), 3120.

Cressey, G. B. (1958). The shatt al-arab basin. *Middle East Journal*, *12*(4), 448–460.

de Morgan, J. (1900). *Délégation en perse: Mémoires.*

Ewaid, S. H., Abed, S. A., & Al-Ansari, N. (2019). Crop water requirements and irrigation schedules for some major crops in southern iraq. *Water*, *11*(4), 756.

Fahrland, E., Jacob, P., Schrader, H., & Hanjo, K. (2020, June). Copernicus dem. product handbook. (2.1 ed.) [Computer software manual].

Isaev, V., & Mikhailova, M. (2009). The hydrography, evolution, and hydrological regime of the mouth area of the shatt al-arab river. *Water resources*, *36*(4), 380–395.

Kennedy, H. (2004). The decline and fall of the first muslim empire. *Der Islam*, *81*(1), 3.

Kennedy, H. (2011). The feeding of the five hundred thousand: cities and agriculture in early islamic mesopotamia. *Iraq*, *73*, 177–199.

Kramers, J. (2012). "al-ubulla". *Encyclopaedia of Islam, Second Edition*. Retrieved 2021-07-06, from `http://dx.doi.org.tudelft.idm.oclc.org/10.1163/1573-3912_islam_SIM_7673`

Lees, G. M., & Falcon, N. (1952). The geographical history of the mesopotamian plains. *The Geographical Journal*, *118*(1), 24–39.

Marine Science Centre: University of Basra in Cooperation with Ministry of Environment. (2011). *The marshes-shatt al-arab- gulf system - status report - volume 1* (Tech. Rep.). UN Environment Programme.

Ministry of Irrigation. (1979). *Shatt al-arab project, feas, rep. draft, studies of salinity problem, part a, text.* Basrah Iraq: Polservies Co.

Ministry of Water Resources. (2018). *Directorate of basra water resources.*

Mosawi, W., & Muter, M. (2019). Application of two frequencies sub-bottom profiler technique for mapping the bottom of shatt al-arab river. *Journal of Basrah Researches ((Sciences))*, *45*(1).

Nelson, H. S. (1962). An abandoned irrigation system in southern iraq. *Sumer*, *18*, 67–72.

Petersen, A. (2018). *Early islamic basrah (iraq)* (Tech. Rep.). Max van Berchem Foundation.

USACE HEC. (2021). Hec-ras river analysis system user's manual [Computer software manual]. Retrieved 2021-10-26, from `https://www.hec.usace.army.mil/software/hec-ras/documentation/HEC-RAS_6.0_Users_Manual.pdf`

USACE Hydrologic Engineering Center. (2021a). Hec-ras 2d user's manual / development of a 2d or combined 1d/2d model / connecting 2d flow areas to 1d hydraulic elements [Computer software manual]. Retrieved 2021-07-19, from `https://www.hec.usace.army.mil/confluence/rasdocs/rasum/`

latest/entering-and-editing-geometric-data/lateral-structures-weirs-gated-spillways-culverts-and-diversion-rating-curves/entering-and-editing-lateral-structure-data

USACE Hydrologic Engineering Center. (2021b). Hec-ras user's manual / entering and editing geometric data / lateral structures (weirs, gated spillways, culverts, and diversion rating curves) / entering and editing lateral structure data [Computer software manual]. Retrieved 2021-07-19, from https://www.hec.usace.army.mil/confluence/rasdocs/rasum/latest/entering-and-editing-geometric-data/lateral-structures-weirs-gated-spillways-culverts-and-diversion-rating-curves/entering-and-editing-lateral-structure-data

Wainwright, H. M., Finsterle, S., Jung, Y., Zhou, Q., & Birkholzer, J. T. (2014). Making sense of global sensitivity analyses. *Computers & Geosciences*, *65*, 84–94.

World Bank Group. (n.d.). *Climate data - historical.* Retrieved 2021-07-29, from https://climateknowledgeportal.worldbank.org/country/iraq/climate-data-historical

Yaseen, Z. M., Al-Juboori, A. M., Beyaztas, U., Al-Ansari, N., Chau, K.-W., Qi, C., ... Shahid, S. (2020). Prediction of evaporation in arid and semi-arid regions: A comparative study using different machine learning models. *Engineering applications of computational fluid mechanics*, *14*(1), 70–89.

A Conversion of DEM

For the Copernicus DEM to be correctly projected in HEC-RAS it first had to be warped using QGIS 3.20.0. To do this, the DEM was added as a raster to a new QGIS project. Then in the main menu under Raster, then Projections, Warp (Reproject) was selected. The Input layer was chosen to be the DEM. The target CPS was EPSG:32639 and the resampling method to use was selected to be Nearest Neighbour. The Output file resolution in target georeferenced units was set to 30 (meters). Then the file was saved and the algorithm run. View figure 17 to view the QGIS warp window and all the used settings.

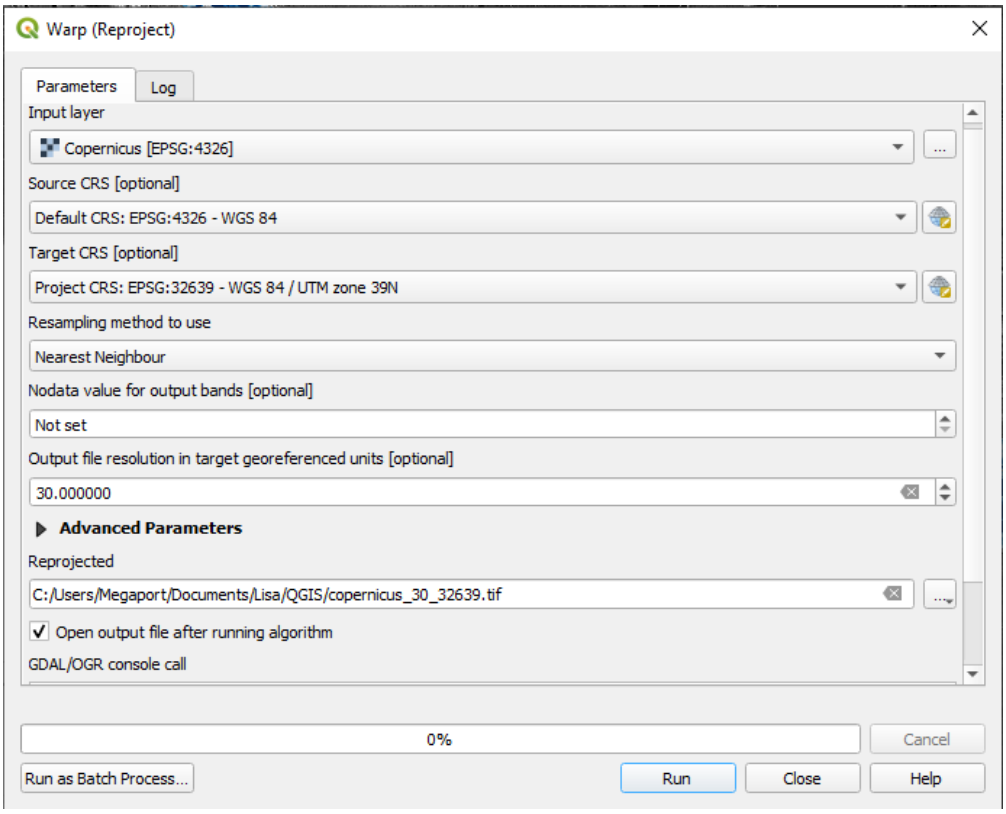

Figure 17: Settings of Warp (Reproject) in QGIS 3.20.0.

B Interpolating River Cross-Sections in HEC-RAS

Further river cross-sections were interpolated using HEC-RAS. This was done using a tool in the Geometric Data Editor, which could be found under Tools in the main menu bar, under XS Interpolation and then by selecting Within a Reach.... The maximum distance between XS's was set to 1000 (meters), under Cut Line GIS Coordinates, Generate for display as perpendicular segments to reach invert was selected, and the Decimal places in interpolates Sta/Elev was set to 0.0 (meaning it will be interpolated with one decimal). View figure 18 for all the settings used.

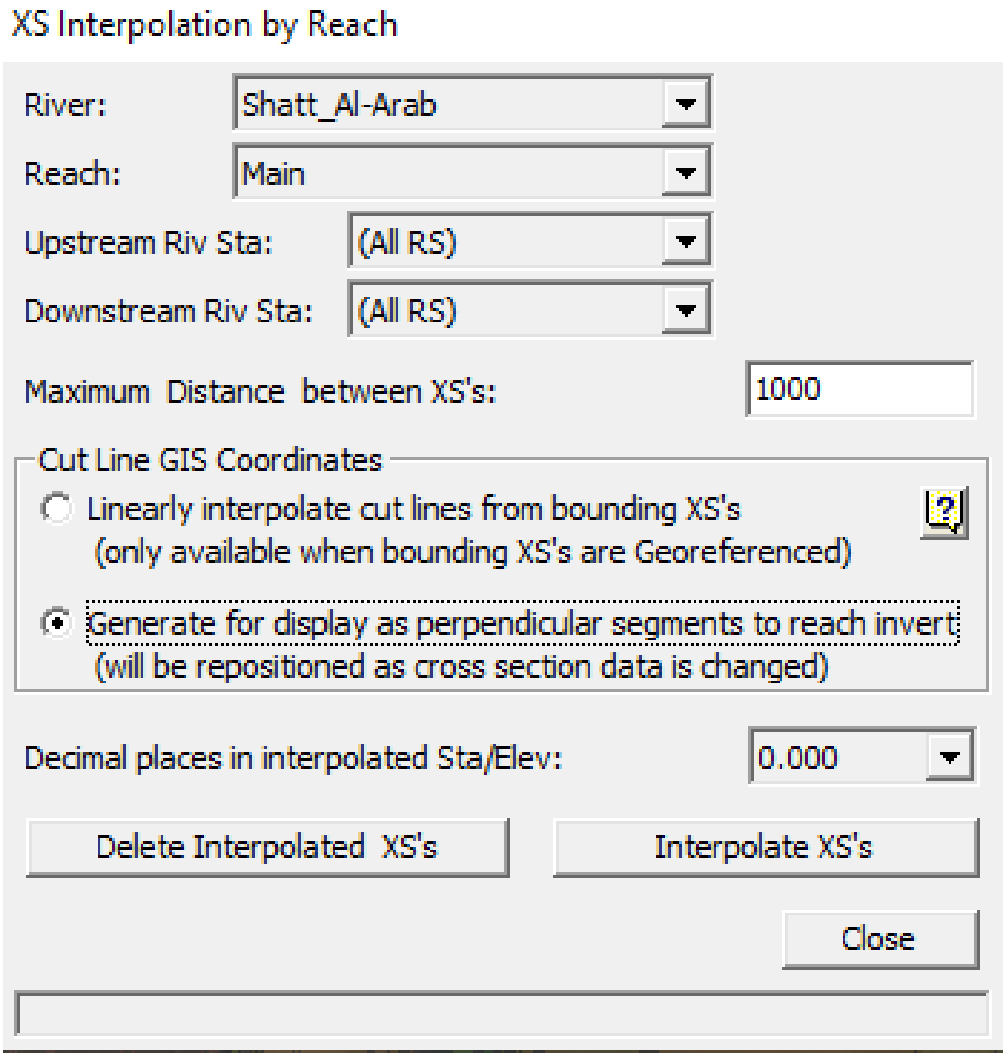

Figure 18: Settings in the XS Interpolation Within a Reach tool in the HEC-RAS Geometric Data Editor.

C Calculating Maximum Time Interval for HEC-RAS

Listing 1: Python code to extract the local maximas and minimas of the flow data and calculate the average time it takes for the hydrograph to reach a peak.

```
import numpy as np
import matplotlib.pyplot as plt
import pandas as pd
from scipy.signal import argrelextrema

# import flow data

euphrates = pd.read_csv('Euphrates_Flow.csv', names=['days', 'flow'])
tigris = pd.read_csv('Tigris_Flow.csv', names=['days', 'flow'])

#sort and reindex data

euphrates = euphrates.sort_values(by='days').reset_index()
tigris = tigris.sort_values(by='days').reset_index()

# Find local peaks

n = 1  # number of points to be checked before and after

euphrates['min'] = euphrates.iloc[argrelextrema(euphrates.flow.values, np.less_equal,
                    order=n)[0]]['flow']
euphrates['max'] = euphrates.iloc[argrelextrema(euphrates.flow.values, np.greater_equal,
                    order=n)[0]]['flow']

tigris['min'] = tigris.iloc[argrelextrema(tigris.flow.values, np.less_equal,
                    order=n)[0]]['flow']
tigris['max'] = tigris.iloc[argrelextrema(tigris.flow.values, np.greater_equal,
                    order=n)[0]]['flow']

# function to calculate the time between the peaks

def time_to_peak(data):
    data_min = data.dropna(subset=['min']).reset_index()
    data_max = data.dropna(subset=['max']).reset_index()
    dif = pd.DataFrame(columns=['difference'])
    for i in range(1, len(data_max)):
        dif1 = data_max.days[i] - data_min.days[data_min.days < data_max.days[i]].max()
        dif1 = pd.DataFrame([dif1], columns=['difference'])
        dif = dif.append(dif1, ignore_index=True)
    print(dif.mean())

# calculate time between the peaks
euphrates_time_to_peak = time_to_peak(euphrates)
tigris_time_to_peak = time_to_peak(tigris)
```

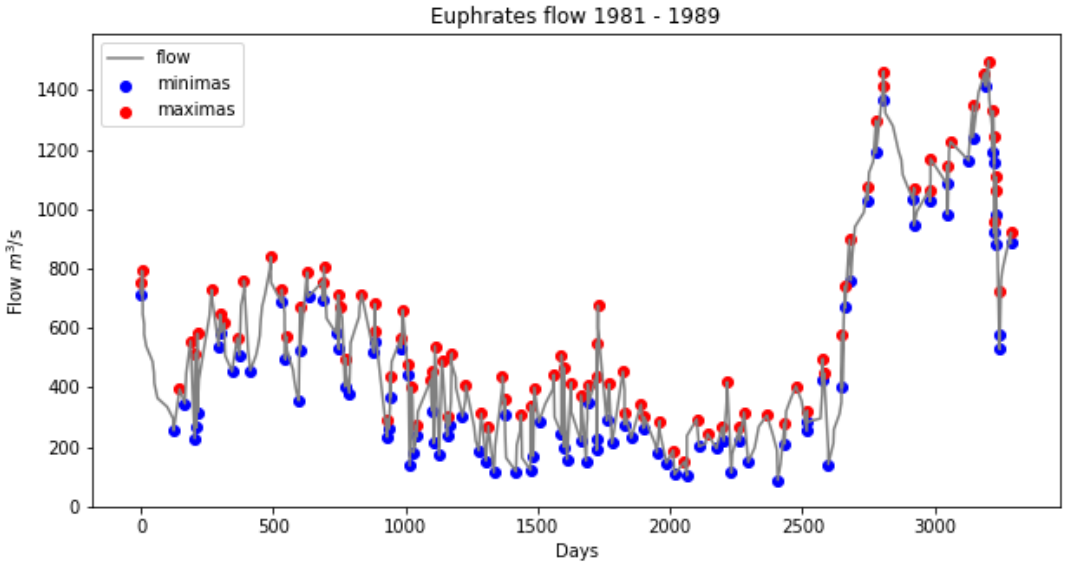

Figure 19: Flow in the Euphrates with local minimum and maximum flow points.

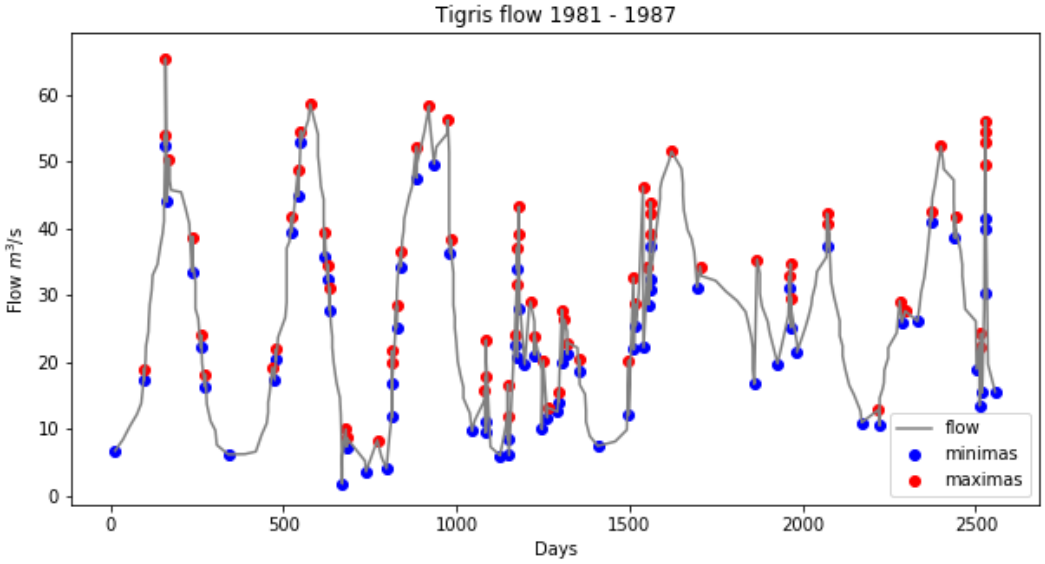

Figure 20: Flow in the Tigris with local minimum and maximum flow points.

D Data Used in Scenario 1 and 2, 01.11.1982

Time	Flow [m^3/s]	Stage [m]	Time	Flow [m^3/s]	Stage [m]
11/1/82 0:00	722.16	2.67	11/1/82 12:00	721.29	2.99
11/1/82 0:30	722.13	2.58	11/1/82 12:30	721.25	2.75
11/1/82 1:00	722.09	2.49	11/1/82 13:00	721.22	2.51
11/1/82 1:30	722.05	2.40	11/1/82 13:30	721.18	2.26
11/1/82 2:00	722.02	2.31	11/1/82 14:00	721.14	2.02
11/1/82 2:30	721.98	2.22	11/1/82 14:30	721.11	1.78
11/1/82 3:00	721.94	2.13	11/1/82 15:00	721.07	1.53
11/1/82 3:30	721.91	2.04	11/1/82 15:30	721.03	1.29
11/1/82 4:00	721.87	1.95	11/1/82 16:00	721.00	1.05
11/1/82 4:30	721.83	1.86	11/1/82 16:30	720.96	0.80
11/1/82 5:00	721.80	1.77	11/1/82 17:00	720.92	0.56
11/1/82 5:30	721.76	1.68	11/1/82 17:30	720.89	0.32
11/1/82 6:00	721.73	1.84	11/1/82 18:00	720.85	0.07
11/1/82 6:30	721.69	2.01	11/1/82 18:30	720.81	-0.17
11/1/82 7:00	721.65	2.17	11/1/82 19:00	720.78	0.05
11/1/82 7:30	721.62	2.33	11/1/82 19:30	720.74	0.27
11/1/82 8:00	721.58	2.50	11/1/82 20:00	720.71	0.48
11/1/82 8:30	721.54	2.66	11/1/82 20:30	720.67	0.70
11/1/82 9:00	721.51	2.83	11/1/82 21:00	720.63	0.92
11/1/82 9:30	721.47	2.99	11/1/82 21:30	720.60	1.14
11/1/82 10:00	721.43	3.15	11/1/82 22:00	720.56	1.35
11/1/82 10:30	721.40	3.32	11/1/82 22:30	720.52	1.57
11/1/82 11:00	721.36	3.48	11/1/82 23:00	720.49	1.79
11/1/82 11:30	721.32	3.24	11/1/82 23:30	720.45	2.01
			11/2/82 0:00	720.41	2.22

Table 9: Flow data from 01.11.1982 for the upstream Shatt Al-Arab boundary condition used in Scenario 1 and 2 and stage data for the downstream Shatt Al-Arab boundary condition used in all scenarios.

E Data Used in Scenario 1 and 2, 01.07.1981

Time	Flow [m^3/s]	Stage [m]	Time	Flow [m^3/s]	Stage [m]
01.07.1981 00:00	460.04	2.67	01.07.1981 12:00	462.17	2.99
01.07.1981 00:30	460.13	2.58	01.07.1981 12:30	462.26	2.75
01.07.1981 01:00	460.22	2.49	01.07.1981 13:00	462.35	2.51
01.07.1981 01:30	460.31	2.40	01.07.1981 13:30	462.44	2.26
01.07.1981 02:00	460.39	2.31	01.07.1981 14:00	462.52	2.02
01.07.1981 02:30	460.48	2.22	01.07.1981 14:30	462.61	1.78
01.07.1981 03:00	460.57	2.13	01.07.1981 15:00	462.70	1.53
01.07.1981 03:30	460.66	2.04	01.07.1981 15:30	462.79	1.29
01.07.1981 04:00	460.75	1.95	01.07.1981 16:00	462.88	1.05
01.07.1981 04:30	460.84	1.86	01.07.1981 16:30	462.97	0.80
01.07.1981 05:00	460.93	1.77	01.07.1981 17:00	463.06	0.56
01.07.1981 05:30	461.02	1.68	01.07.1981 17:30	463.15	0.32
01.07.1981 06:00	461.10	1.84	01.07.1981 18:00	463.23	0.07
01.07.1981 06:30	461.19	2.01	01.07.1981 18:30	463.32	-0.17
01.07.1981 07:00	461.28	2.17	01.07.1981 19:00	463.41	0.05
01.07.1981 07:30	461.37	2.34	01.07.1981 19:30	463.50	0.27
01.07.1981 08:00	461.46	2.50	01.07.1981 20:00	463.59	0.48
01.07.1981 08:30	461.55	2.66	01.07.1981 20:30	463.68	0.70
01.07.1981 09:00	461.64	2.83	01.07.1981 21:00	463.77	0.92
01.07.1981 09:30	461.73	2.99	01.07.1981 21:30	463.86	1.14
01.07.1981 10:00	461.81	3.15	01.07.1981 22:00	463.94	1.35
01.07.1981 10:30	461.90	3.32	01.07.1981 22:30	464.03	1.57
01.07.1981 11:00	461.99	3.48	01.07.1981 23:00	464.12	1.79
01.07.1981 11:30	462.08	3.24	01.07.1981 23:30	464.21	2.01
			02.07.1981 00:00	464.30	2.23

Table 10: Flow data from 01.07.1981 for the upstream Shatt Al-Arab boundary condition used in Scenario 1 and 2 and stage data for the downstream Shatt Al-Arab boundary condition used in all scenarios.

F Coast Location in Scenario 2 and 4

Figure 21: The red dots indicate the interpolated coast location from figure 6 and the alternative coast line utilised in scenario 2 as explained in section 2.6.2. The red dashed line indicates the ridge system area.

G QGIS Post-Processing Using Zonal Statistics

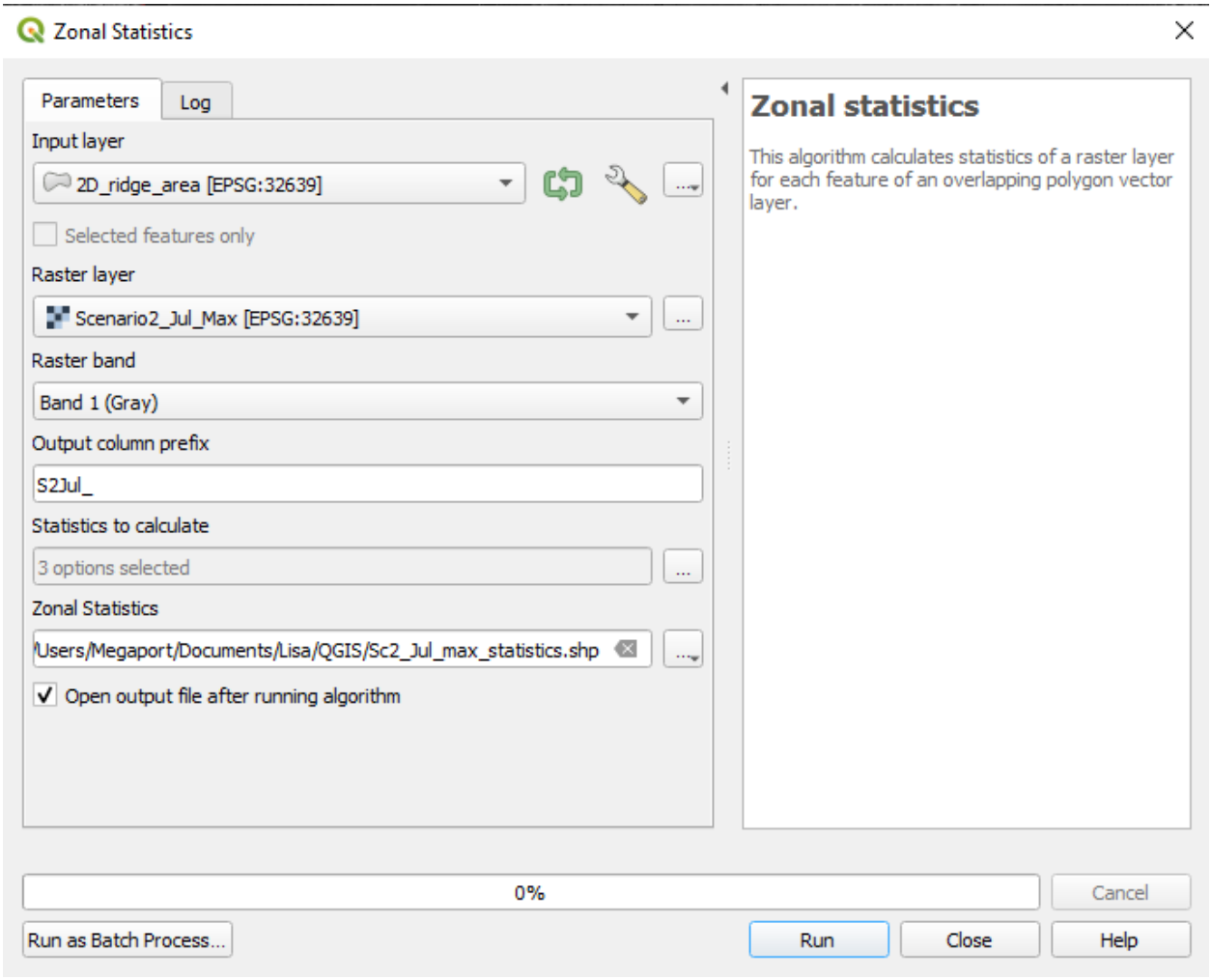

Figure 22: Settings used in the zonal statistics tool in QGIS for data post-processing.

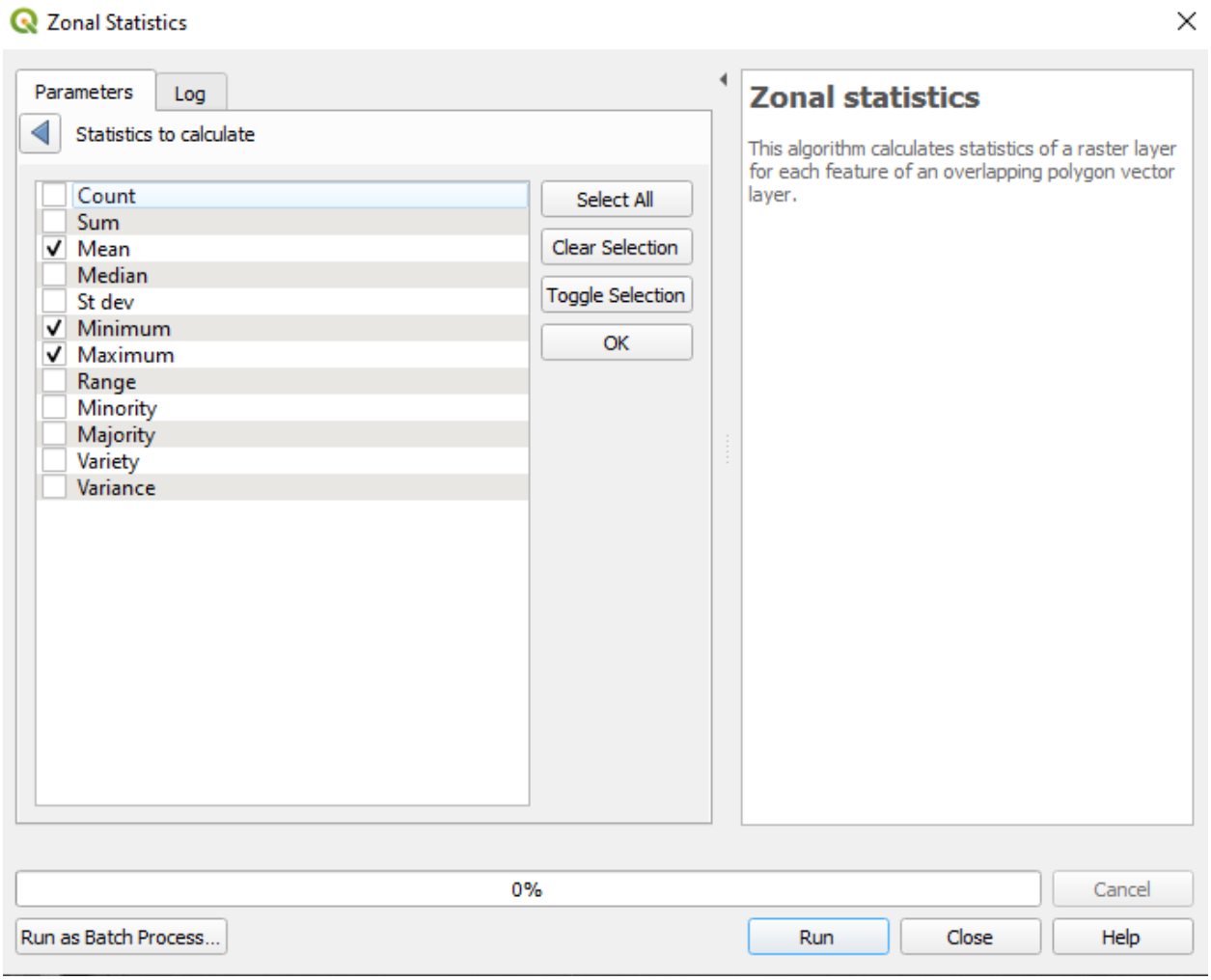

Figure 23: The statistics calculated with the zonal statistics tool in QGIS.

H Scenario 3, May, Water Surface Profile

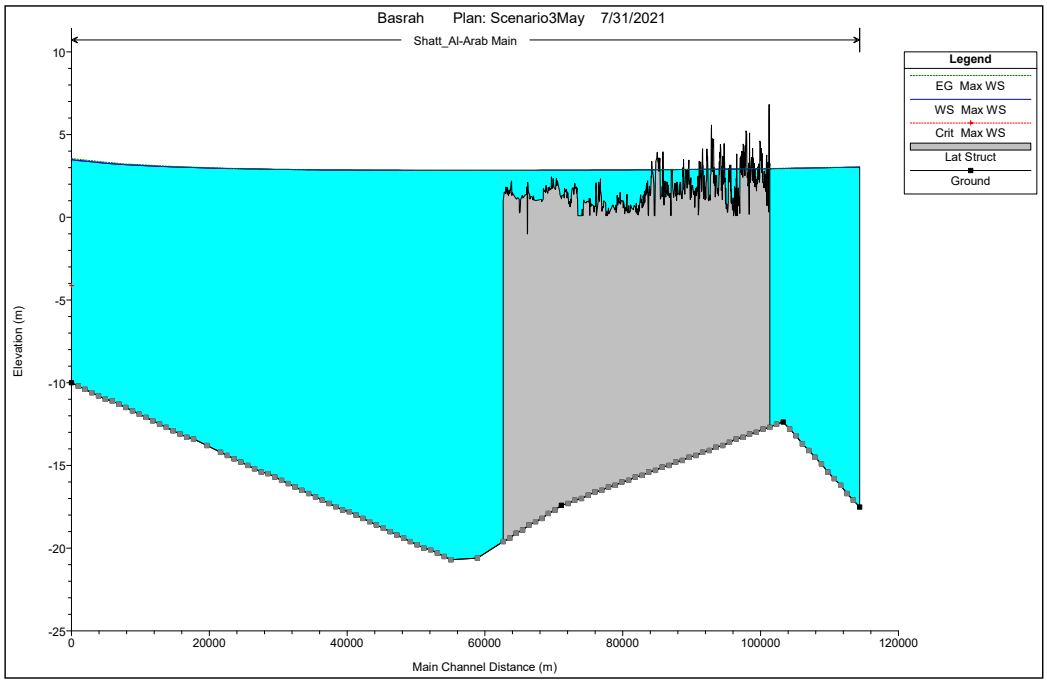

Figure 24: The water surface in the Shatt Al-Arab in Scenario 3 run with the May flow data. The most downstream point is at 0 m main channel distance and increases upstream.

I Terrain Profile Along Lateral Structure

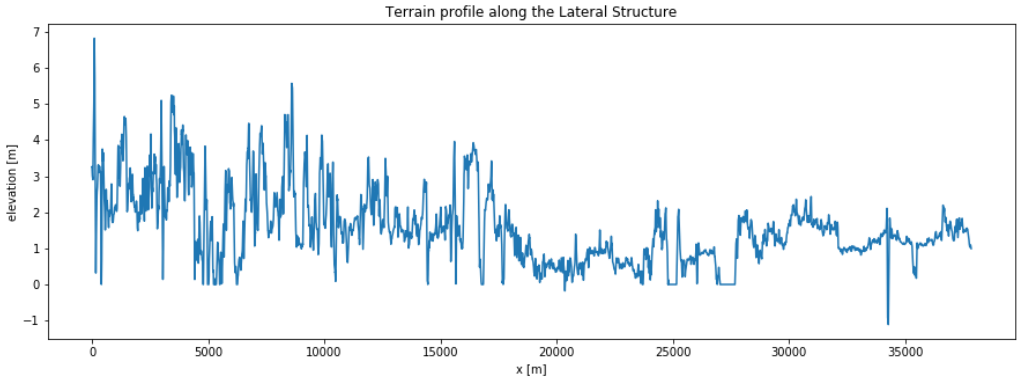

Figure 25: Terrain profile along the right river bank by the ridge area. The exact location is visualised in figure 3 and labeled as 'Lateral Structure' The distance is measured from up- to downstream.

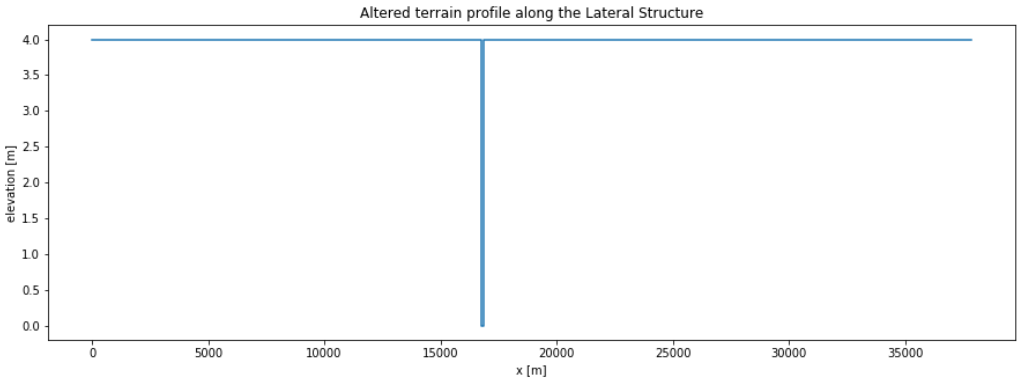

Figure 26: Altered terrain profile along the right river bank by the ridge area as utilized in the sensitivity analysis for the flow from the river into the ridge area. The exact location of the terrain is visualised in figure 3 and labeled as 'Lateral Structure'. The distance is measured from up- to downstream.

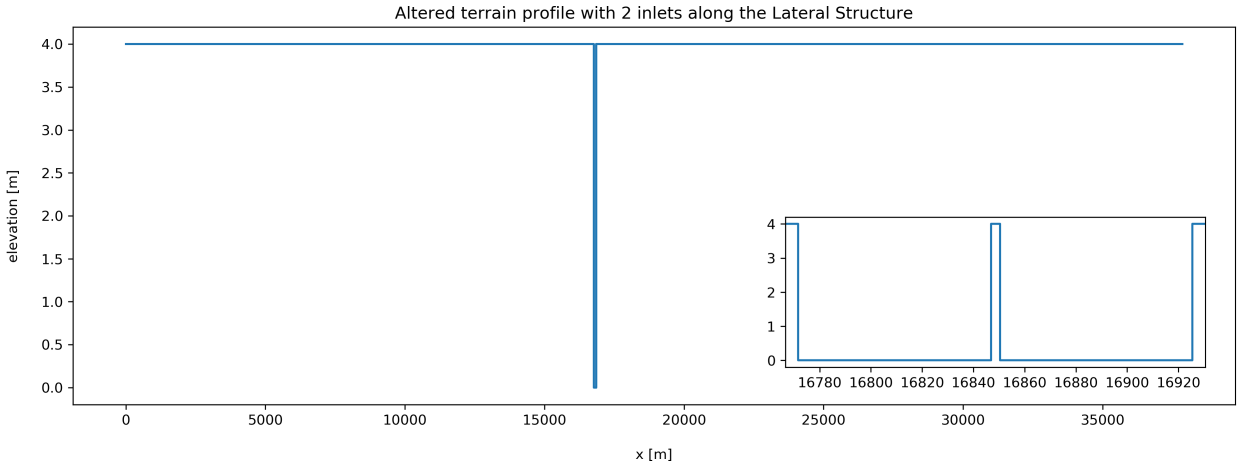

Figure 27: Altered terrain profile along the right river bank by the ridge area with 2 inlets as utilized in the sensitivity analysis for the flow from the river into the ridge area. The exact location of the terrain is visualised in figure 3 and labeled as 'Lateral Structure'. The distance is measured from up- to downstream.

J HEC-RAS Modelling Files

All the files used and created in the process of this study can be requested from Dr. Ir. Maurits Ertsen at M.W.Ertsen@tudelft.nl.